THE JOURNAL OF PHYSICAL CHEMISTRY B

Article

Cite This: J. Phys. Chem. B 2018, 122, 40−53

pubs.acs.org/JPCB

pH-Dependent Singlet O_2 Oxidation Kinetics of Guanine and 9-Methylguanine: An Online Mass Spectrometry and Spectroscopy Study Combined with Theoretical Exploration

Wenchao Lu,[†,‡] Yan Sun,[†,‡] Wenjing Zhou,[†] and Jianbo Liu*[,†,‡]

[†]Department of Chemistry and Biochemistry, Queens College of the City University of New York, 65-30 Kissena Boulevard, Queens, New York 11367, United States

[‡]Ph.D. Program in Chemistry, The Graduate Center of the City University of New York, 365 Fifth Avenue, New York, New York 10016, United States

Supporting Information

ABSTRACT: We report a kinetic and mechanistic study on the title reactions, in which $^1O_2$ was generated by the reaction of H_2O_2 with Cl_2 and bubbled into an aqueous solution of guanine and 9-methylguanine (9MG) at different pH values. Oxidation kinetics and product branching ratios were measured using online electrospray ionization mass spectrometry coupled with absorption and emission spectrophotometry, and product structures were determined by collision-induced dissociation (CID) tandem mass spectrometry. Experiments revealed strong pH dependence of the reactions. The oxidation of guanine is noticeable only in basic solution, while the oxidation of 9MG is weak in acidic solution, increases in neutral solution, and becomes intensive in basic solution. 5-Guanidinohydantoin (Gh) and spiroiminodihydantoin (Sp) were detected as the major oxidation products of guanine and 9MG, and Sp became dominant in basic solution. A reaction intermediate was captured in mass spectra, and assigned to *gem*-diol on the basis of CID measurements. This intermediate served as the precursor for the formation of Gh. After taking into account solution compositions at each pH, first-order oxidation rate constants were extracted for individual species: that is, $3.2-3.6 \times 10^7$ M^{-1} s^{-1} for deprotonated guanine, and 1.2×10^6 and $4.6-4.9 \times 10^7$ M^{-1} s^{-1} for neutral and deprotonated 9MG, respectively. Guided by approximately spin-projected density-functional-theory-calculated reaction potential energy surfaces, the kinetics for the initial $^1O_2$ addition to guanine and 9MG was evaluated using transition state theory (TST). The comparison between TST modeling and experiment confirms that $^1O_2$ addition is rate-limiting for oxidation, which forms endoperoxide and peroxide intermediates as determined in previous measurements of the same systems in the gas phase.

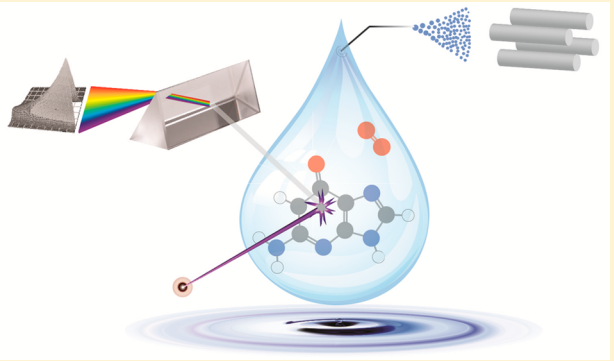

1. INTRODUCTION

Oxidatively generated damage of DNA nucleobases gives rise to mutagenesis, DNA−protein cross-linking, and cellular lethality.[1−3] One category of such damage is caused by electronically excited singlet oxygen (O_2, $a^1\Delta_g$) which is produced by photosensitization and/or a range of enzymatic and nonenzymatic reactions in live organisms.[4] Of the four DNA nucleobases (i.e., adenine, thymine, guanine, and cytosine), guanine (G) is the most susceptible to $^1O_2$ oxidation. The oxidation mechanism of guanine nucleoside is outlined in Scheme 1.[5−17] In brief, deoxyguanosine (dGuo) is attacked by $^1O_2$ on the imidazole ring for a [4 + 2] cycloaddition, forming a transient endoperoxide that quickly converts to a hydroperoxide 8-OOHdGuo. 8-OOHdGuo within DNA is mainly reduced to 8-oxo-7,8-dihydrodeoxyguanosine (OdGuo). Free 8-OOHdGuo or that in short oligonucleotides, on the other hand, undergoes dehydration to form oxidized 8-oxo-7,8-dihydrodeoxyguanosine ($OdGuo^{ox}$) and then rehydration to form 5-hydroxy-8-oxo-7,8-dihydrodeoxyguanosine (5-OHOdGuo). Subsequent conversions from 5-OHOdGuo are pH-dependent. Under basic conditions, 5-OHOdGuo goes through an acyl shift to produce spiroiminodihydantoin (dSp);[18] whereas under acidic conditions, the formation of a *gem*-diol intermediate via the addition of a water to 5-OHOdGuo becomes predominant. Ring-opening at the N1−C6 bond of *gem*-diol, accompanied by an intramolecular proton transfer, leads to a 4-carboxydGh. Decarboxylation of the latter results in the formation of 5-guanidinohydantoin (dGh).[9,19] In addition, OdGuo may react with a second $^1O_2$ and form 5-hydroperoxy-8-oxo-7,8-dihydrodeoxyguanosine (5-OOHOdGuo), followed by reduction to 5-OHOdGuo or decarboxylation to oxidized 5-guanidinohydantoin (dGh^{ox}).[14]

Received: September 25, 2017
Revised: November 28, 2017
Published: November 29, 2017

DOI: 10.1021/acs.jpcb.7b09515
J. Phys. Chem. B 2018, 122, 40−53

Scheme 1. $^1O_2$ Oxidation Pathways of dGuo

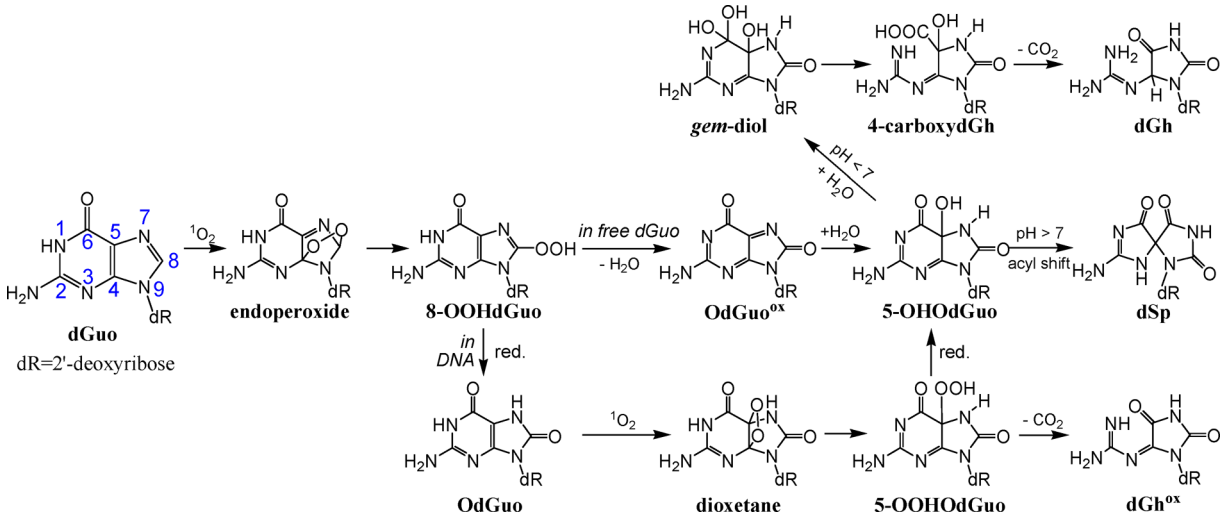

Detection of reaction intermediates is crucial for verifying the oxidation mechanism of guanine and the pathways to the end products. One such experiment, from which the cycloaddition with $^1O_2$ was extrapolated, was reported by the Foote group.[5,8] They detected an endoperoxide from the photooxidation of 2′,3′,5′-*O*-(*tert*-butyldimethylsilyl)-8-methylguanosine in CD_2Cl_2 at −78 °C using NMR spectroscopy, and found that the 8-methyl-substituted endoperoxide decomposed back to reactants once it warmed up to −30 °C. Attempts to observe the formation of endoperoxide from guanine or other guanosine derivatives (where the labile 8-H is preserved) all failed, even at a temperature down to −100 °C.[8,20] On the basis of the similar low-temperature NMR characterization, 5-OOHOG and its reduction product 5-OHOG were detected at −60 °C in the $^1O_2$ oxidation of 2′,3′,5′-tris(*O*-*tert*-butyldimethylsilyl)-8-oxo-7,8-dihydroguanosine,[10] and 5-OHOG rearranged to Sp at room temperature. Recently, we reported the detection of endoperoxide and 8-peroxide intermediates in the gas-phase reactions of $^1O_2$ with protonated and deprotonated guanine and 9-methylguanine (9MG) at room temperature, using guided-ion-beam scattering tandem mass spectrometry.[21,22] Our experiment determined that the $^1O_2$ addition to guanine and 9MG ions is exothermic and has no barriers above the reactants.

Computational modeling of guanine oxidation has assisted the interpretation of experimental results and refined the oxidation mechanism. By using a compilation of density functional theory (DFT) and post-Hartree−Fock methods, Schlegel, Burrows, and co-workers proposed that $^1O_2$ follows a stepwise addition to guanine instead of a concerted [4 + 2] addition, and the initial adduct may be characterized as a zwitterionic 8-peroxide.[23] The same group also calculated the reaction potential energy surfaces (PESs) from the 5-OHOG intermediate to Sp and Gh using B3LYP coupled with the IEF-PCM solvation model, from which the pH dependence of product branching ratios was predicted.[19,24] A stepwise $^1O_2$-addition mechanism was also reported in a quantum mechanics/molecular mechanics study on the $^1O_2$ oxidation of a 13-base-pair poly(dG-dC) by Dumont et al.,[25,26] and the B-helical DNA environment was found to be able to stabilize the nascent 8-peroxide. To obtain insights into our experimental findings concerning the influences of protonation, deprotonation, and N9-substitution on guanine oxidation, we have simulated the gas-phase guanine and 9MG oxidation using the DFT, MP2, CCSD(T), and CASSCF theories and quasi-classical direct dynamics trajectories.[21,22] Our work indicated that both protonated and deprotonated guanine form 5,8-endoperoxides during the oxidation. Protonated 9MG also favors the formation of a 5,8-endoperoxide; by contrast, deprotonated 9MG involves a stepwise $^1O_2$ addition starting with the formation of an 8-peroxide, followed by interconversion to a 4,8-endoperoxide.[21,22] Note that the N9-methyl group of 9MG mimics the attachment of a sugar group to the guanine nucleoside, and 9MG has pK_a values[27] and the nucleobase conformation[28] resembling those of guanosine.[28−30] Therefore, 9MG could be used as a guanosine prototype compound, and the results of 9MG are more biochemically relevant.

Our gas-phase study of guanine and 9MG was centered on early-stage reaction dynamics and the formation of endoperoxide/peroxide intermediates. The present work has extended our investigation from the gas phase to solution, with the focus on the late-stage kinetics evolving from endoperoxides/peroxides and the formation of end products. Most of the solution-phase $^1O_2$ oxidation experiments were carried out using the photosensitization method where a sensitizer is excited on exposure to UV−vis light and transfers its excitation energy to $^3O_2$ (type II sensitization).[17,31] One issue with using the photosensitized oxidation method is that the excited sensitizer may generate radicals via electron transfer (type I sensitization),[17,31] and the resulting radicals compete with $^1O_2$ for substrates, affecting measurements of $^1O_2$ kinetics. Thermolysis of naphthalene endoperoxide may be used as an alternative $^1O_2$ source. This method requires adding naphthalene endoperoxide to reaction solution, and the concentration of reacting $^1O_2$ is difficult to determine, making it less ideal for kinetic experiments.[6,32] In the present work we adopted a chemical $^1O_2$ generator,[33,34] which is capable of eliminating radicals and in the meantime delivers a constant concentration of $^1O_2$. The $^1O_2$ generator was integrated into a homemade solution-phase reaction system, which was developed to facilitate real-time electrospray ionization mass spectrometry (ESI MS) and spectroscopy measurements.[35,36] Online ESI MS serves as a sensitive technique to detect reaction products at the micromolar scale, and allows detection of short-lived intermediates that may not survive separation and/or off-line analysis. Coupled with absorption and emission spectroscopy, this system not only measures the oxidative decay of reactants but also distinguishes individual products. Capitalizing on this apparatus, we have

DOI: 10.1021/acs.jpcb.7b09515
J. Phys. Chem. B 2018, 122, 40−53

measured the $^1O_2$ oxidation of guanine and 9MG at pH = 3.0, 7.0, and 10.0, respectively.

2. EXPERIMENTAL AND COMPUTATIONAL DETAILS

All chemicals were used without further purification. Solutions of guanine (BioUltra grade, Sigma-Aldrich) and 9MG (≥98%, Chemodex) were prepared at a concentration of 0.03 mM in citric acid/NaOH/NaCl buffer (pH 3.0, Fluka), phosphate buffer (pH 7.0, Alfa Aesar), and borax/NaOH buffer (pH 10.0, Fluka), respectively. The maximum UV absorbances of these solutions fell within the range 0.1−1.0, and the absorbances at the fluorescence excitation wavelength (290 nm) were less than 0.05. Under these conditions, both absorbances and fluorescence intensities are linearly related to reactant concentrations. For MS measurements, solutions of guanine and 9MG were prepared at 0.05−0.5 mM, and their pH was adjusted to the desired value using HCl or NaOH solution to avoid the suppression of reactants and products ESI by buffer ions.

2.1. $^1O_2$ Generation and Online Spectroscopy. $^1O_2$ was generated by the reaction $H_2O_2 + Cl_2 + 2KOH \rightarrow {}^1O_2/{}^3O_2 + 2KCl + 2H_2O$.[37,38] In brief, 10.5 mL of 8 M KOH (85%, Alfa Aesar) was slowly added to 20 mL of aqueous H_2O_2 (35 wt %, Alfa Aesar) in a sparger (**1**) held at −17 °C as shown in Figure 1. The resulting mixture was degassed quickly. 4.4 sccm of Cl_2 (~99.5%, Sigma-Aldrich) was diluted in 96 sccm of He and bubbled through the H_2O_2/KOH slush. All of the Cl_2 reacted with H_2O_2 to produce a mixture of $^1O_2$, $^3O_2$, and water. Gas products passed through a −70 °C cold trap (**2**) to remove water vapor. Only $^1O_2$, $^3O_2$, and He remained in the gas products. The concentration of $^1O_2$ in the gas phase was determined by measuring $^1O_2$ emission ($a^1\Delta_g \rightarrow X^3\Sigma_g^-$)[39] at 1270 nm in an optical emission cell (**3**). The emission was collimated by a plano-convex lens, and passed through an optical chopper (**4**, Stanford Research System SR540) and a 1270 nm interference filter. The chopped emission was focused by another plano-convex lens into a thermoelectrically cooled InGaAs detector (**5**, Newport 71887 detector with 77055 TE-cooler controller), and the detector signal was processed by a lock-in amplifier (Stanford Research System SR830).

The gas mixture was then bubbled into a reaction vessel (**6**) containing the aqueous solution of guanine or 9MG. The entire reaction apparatus was continuously evacuated by a mechanical pump (**7**), and the pressure within **6** was maintained at 25 Torr

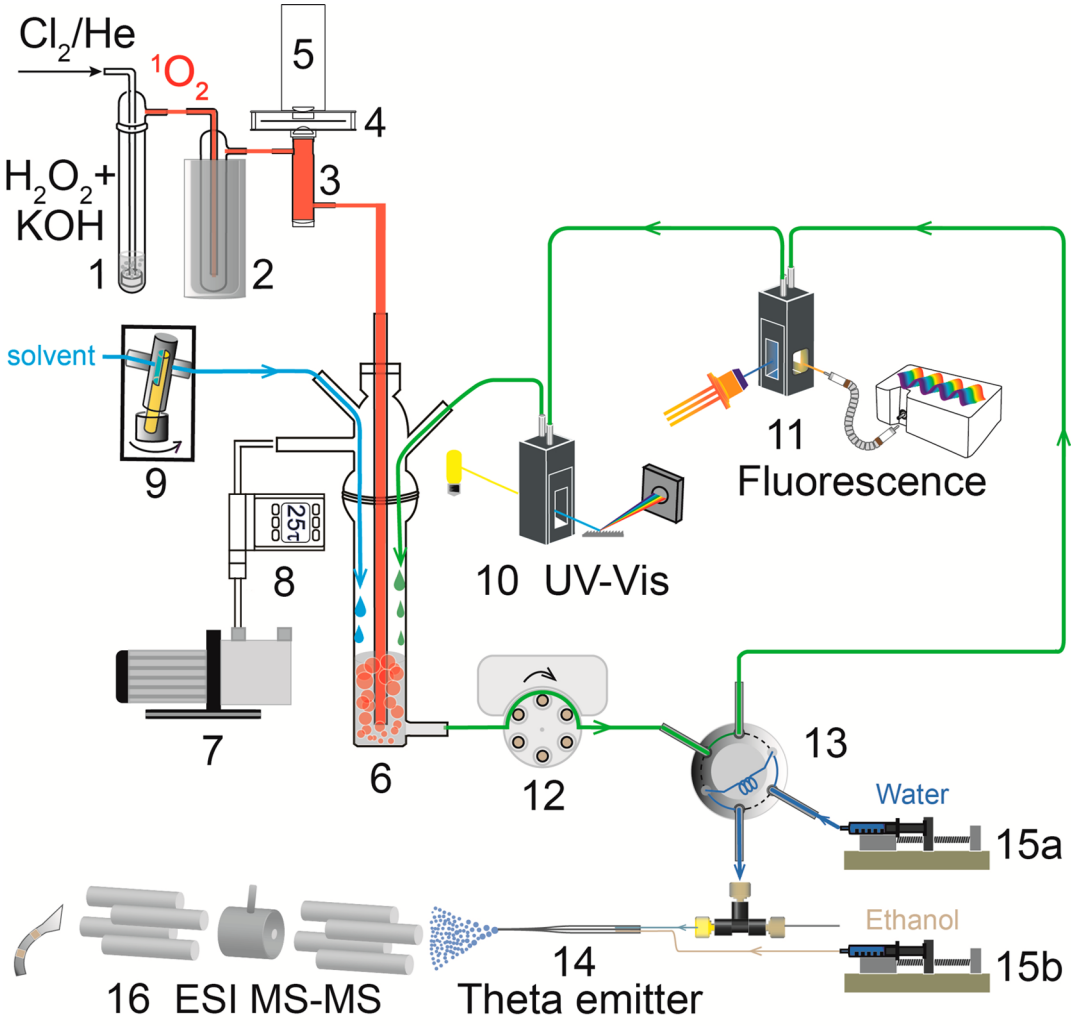

Figure 1. Online reaction monitoring using ESI mass spectrometry and absorption/emission spectroscopy: (1) sparger, (2) cold trap, (3) emission cell, (4) optical chopper, (5) InGaAs photodetector, (6) reaction vessel, (7) mechanical pump, (8) pressure relay, (9) piston pump, (10) UV−vis spectrometer, (11) fluorometer, (12) peristaltic pump, (13) two-position switching valve, (14) theta-ESI emitter, (15a,b) syringe pumps, and (16) ESI MS.

DOI: 10.1021/acs.jpcb.7b09515
J. Phys. Chem. B 2018, 122, 40−53

using a pressure relay (**8**, Cole-Parmer 00244OW). The pumping continuously transported fresh $^1O_2$ to the reaction solution and removed quenched O_2 from the system by gas flow, so that quasi-steady-state [$^1O_2$] could be achieved in the solution.[36] The calibration of [$^1O_2$] in the solution (Figure S1) is available in the Supporting Information, along with the description of the calibration methodology. To compensate for the evaporation loss of water at the reduced pressure, makeup solvent was replenished into **6** through a rotary piston pump (**9**) to keep the solution volume constant during the reaction.

The online reaction monitoring system was reported before.[36] The original setup consisted of only a UV−vis spectrometer (**10**, Ocean Optics USB4000 diode-array spectrometer and USB-ISS-UV/vis light source) and an ESI MS (**16**). A difficulty in the measurement of guanine oxidation in basic solution is that the UV−vis absorption bands of guanine overlap with those of oxidation products, rendering absorption spectroscopy incapable of detecting oxidation. On the other hand, guanine has unique fluorescence emission under basic conditions. In the present work, we have upgraded the system by adding a miniature fluorometer (**11**, Ocean Optics Flame-S spectrometer with 290 nm LED excitation source), and used fluorescence in parallel with UV−vis absorption to monitor reaction progress. The reactant solution was continuously circulated to **10** and **11** in series using a peristaltic pump (**12**). Absorption and fluorescence spectra were recorded at an interval of 20 s using OceanView 1.5.2 software. The integration time for fluorescence was set to 10 s, and each spectrum was averaged over two consecutive measurements. The integration time for absorption was set to 40 ms.

2.2. Online ESI MS and Collision-Induced Dissociation Tandem MS. The sampling loop for MS measurement was realized by a two-position switching valve (**13**). For each MS measurement, the valve loaded 150 μL of sample solution, and was then switched to the MS injection mode. A theta-glass capillary (**14**, 40 μm o.d. × 20 μm i.d. at the tip, pulled by Sutter Instrument P-2000) was used as an ESI emitter.[40−42] One channel of the theta capillary was connected to the sampling loop, and the solution was delivered to the spray by a syringe pump (**15a**) at the speed of 0.01 mL/h. The other channel was filled with ethanol, driven by another syringe pump (**15b**) at the speed of 0.04 mL/h. Two solutions mixed at the tip of the ESI emitter. Addition of ethanol to electrospray not only reduced the amount of the sample solution needed for MS analysis, but also avoided the occurrence of corona discharge[43] that would otherwise inhibit ESI of aqueous solution in the negative ion mode. The ESI emitter was held at ±2.3 kV relative to ground for producing positively and negatively charged species, respectively. Neutral reaction solutions were measured in the positive ion mode by adding 10 mM HCl to the ethanol solvent. MS spectra were recorded at an interval of 30−60 s for a duration of 1 h.

MS measurement was carried out on a homemade guided-ion-beam tandem mass spectrometer.[44] The instrument consists of an ESI ion source, a radio frequency (rf) hexapole ion guide, a quadrupole mass filter, an rf octopole ion guide surrounded by a scattering cell, a second quadrupole mass filter, and a pulse-counting electron multiplier. Both quadrupoles used Extrel 9.5 mm diameter trifilter rods and were operating at 2.1 MHz with a detectable m/z range 1−500. In regular MS measurements, ions were guided to the first quadrupole mass analyzer for mass analysis, and the second quadrupole mass analyzer was rendered to an rf-only mode, passing all of the ions to the electron multiplier detector.

To identify the structures of product ions, collision-induced dissociation (CID) MS/MS was carried out. In the CID experiment, the first quadrupole was used to select product ions of interest. Mass-selected ions were collected into the octopole ion guide, which trapped ions in the radial direction. In addition to rf voltages, direct current (dc) bias voltage of variable polarity and amplitude was applied to the octopole ion guide to determine initial kinetic energy distributions of the primary ions using retarding potential analysis.[45] The dc bias voltage also allowed control of the kinetic energy of the ions in the laboratory frame (E_{lab}), thereby setting the collision energy (E_{col}) between the ions and collision gas in the center-of-mass frame, that is, $E_{col} = E_{lab} \times m_{neutral}/(m_{ion} + m_{neutral})$, where $m_{neutral}$ and m_{ion} are the masses of neutral collision gas and ions, respectively. The octopole runs through the scattering cell filled with xenon gas (99.995%, Spectra Gases). The cell pressure was set to 0.20 mTorr, measured by a Baratron capacitance manometer (MKS 690 head and 670 signal conditioner). CID was measured at E_{col} of 1.5 eV. Fragment ions and unreacted primary ions drifted to the end of the octopole, and were mass analyzed by the second quadrupole and counted by the electron multiplier.

The entire experiment was repeated multiple times. The data presented are averages of several complete data sets collected over 4 months. To determine if reactions were $^1O_2$-specific, control experiments were conducted using pure $^3O_2$ under otherwise the same conditions.

2.3. Computational Details. Geometries of reactants, products, intermediates, and transition states (TSs) were optimized at the ωB97XD level of theory (a hybrid GGA with dispersion correction)[46] coupled with the SMD solvation model[47] and the 6-31+G(d,p) basis set. All possible conformers arising from guanine and 9MG in different ionization states were computed, and their global minima were used as the starting geometries for reaction PESs. Zero-point energies were scaled by a factor of 0.975[48] in the calculations of thermal corrections at 298 K. All TSs were verified to be first-order saddle points, with the vibrational mode associated with an imaginary frequency corresponding to the anticipated reaction pathway. Intrinsic reaction coordinate (IRC) trajectories were carried out to confirm the reactant and product minima connected through the TSs. Energies for PESs were refined using SMD-ωB97XD/aug-cc-pVQZ single point calculations. All of the calculations were carried out using Gaussian 09 D.01.[49]

$^1O_2$ is well-known for its computational difficulty. Due to the associated mixed open- and closed-shell characters,[50] closed-shell calculations fail to produce an accurate value of $^1O_2$ excitation energy; on the other hand, open-shell, broken-symmetry calculations bring about significant spin-contamination from the triplet state that affects the results, too. A common workaround to this problem is to add the experimental excitation energy of $^1O_2$ (94.6 kJ/mol)[39] to the calculated energy of $^3O_2$. However, spin-contamination exists not only for the $^1O_2$ reactant but also in reaction intermediates and TSs. A more rigorous approach is based on multireferential calculations. For example, Marchetti et al. have used the CASPT2//SA-CASSCF method to study the addition of $^1O_2$ to guanine and histidine.[51] We have mapped out 2D-PESs for the $^1O_2$ addition to 9MG using CASSCF.[22] It turns out that the CASSCF PESs resembled those obtained using B3LYP and ωB97XD. Particularly, late-stage intermediates and TSs

DOI: 10.1021/acs.jpcb.7b09515
J. Phys. Chem. B 2018, 122, 40−53

(after the formation of endoperoxide) are all closed-shell and dominated by single electronic states, according to their T1 diagnostic values which are below the 0.02 threshold.[52] In other words, spin-contamination would likely not become a serious issue at the late stage of the $^1O_2$ reactions with guanine and 9MG when wavefunctions become stable in restricted calculations. In view of these findings, in this work we have chosen to adopt a more strategic approach based on Yamaguchi's approximate spin-projection[53,54] to correct for spin-contamination for early-stage PESs. The spin-projected electronic energy for the open-shell singlet state (E^{AP}) was calculated using eq 1,[53] where E refers to the electronic energy, with the superscript AP representing the approximately spin-projected singlet state, BS the open-shell, broken-symmetry singlet state, and HS the higher-spin (triplet) state. $\langle \mathbf{S}^2 \rangle$ indicates the spin-contamination.

$$E^{AP} = \frac{E^{BS}\langle \mathbf{S}^2 \rangle^{HS} - E^{HS}\langle \mathbf{S}^2 \rangle^{BS}}{\langle \mathbf{S}^2 \rangle^{HS} - \langle \mathbf{S}^2 \rangle^{BS}} \quad (1)$$

All energies were calculated at SMD-ωB97XD/aug-cc-pVQZ//SMD-ωB97XD/6-31+G(d,p). The so-calculated $^1O_2$ excitation energy is 96.5 kJ/mol, in a good agreement with the experimental value of 94.6 kJ/mol. Schlegel and co-workers assessed the approximate spin-projection approach at the ωB97XD level using $^1O_2$-induced guanine–lysine cross-linking as a test system, and found the results comparable to CCSD(T).[23] We have recently used this method to construct reaction PESs for the gas-phase experiment of $^1O_2$ with cystine ions.[55] It has been shown that, with careful benchmark tests, this method could be used to produce correct reaction PESs.

3. RESULTS AND DISCUSSION

3.1. $^1O_2$ Oxidation of Guanine. The oxidation of guanine was minor, if there was any, at pH 3.0 and 7.0, as revealed by real-time mass spectra (Figures S2 and S3 in the Supporting Information, in which m/z 152 corresponds to $[G + H]^+$ and all the rest of the ion peaks were found to arise from background). The relative abundances of all ion peaks have remained constant throughout the 1 h reaction. UV–vis absorption measurements (spectra now shown) did not show any changes, either.

The reaction became remarkable at pH 10.0, leading to the formation of products at m/z 154, 156, 182, and 200 (highlighted in the mass spectra of Figure 2a). All products were scrutinized to be $^1O_2$-specific. The structures of these product ions were characterized by CID MS/MS, and the results are given in Figure 2b. The m/z 182 and 156 signals are attributed to deprotonated Sp and Gh, respectively. The assignments were based on the comparison of our negative CID product mass spectra with the CID mass spectra of the same compounds reported in the positive ion mode.[9,56−58] The molecular ion peaks of $[Sp - H]^-$ and $[Gh - H]^-$ and their major fragmentation ions could match their counterpart peaks at $[m/z + 2]$ in the positive ESI MS of $[Sp + H]^+$[56−58] and $[Gh + H]^+$,[9] respectively. In addition, major fragments of $[Sp - H]^-$ and $[Gh - H]^-$ could all be explained by the partial structures shown in the inset of Figure 2b. We have attributed

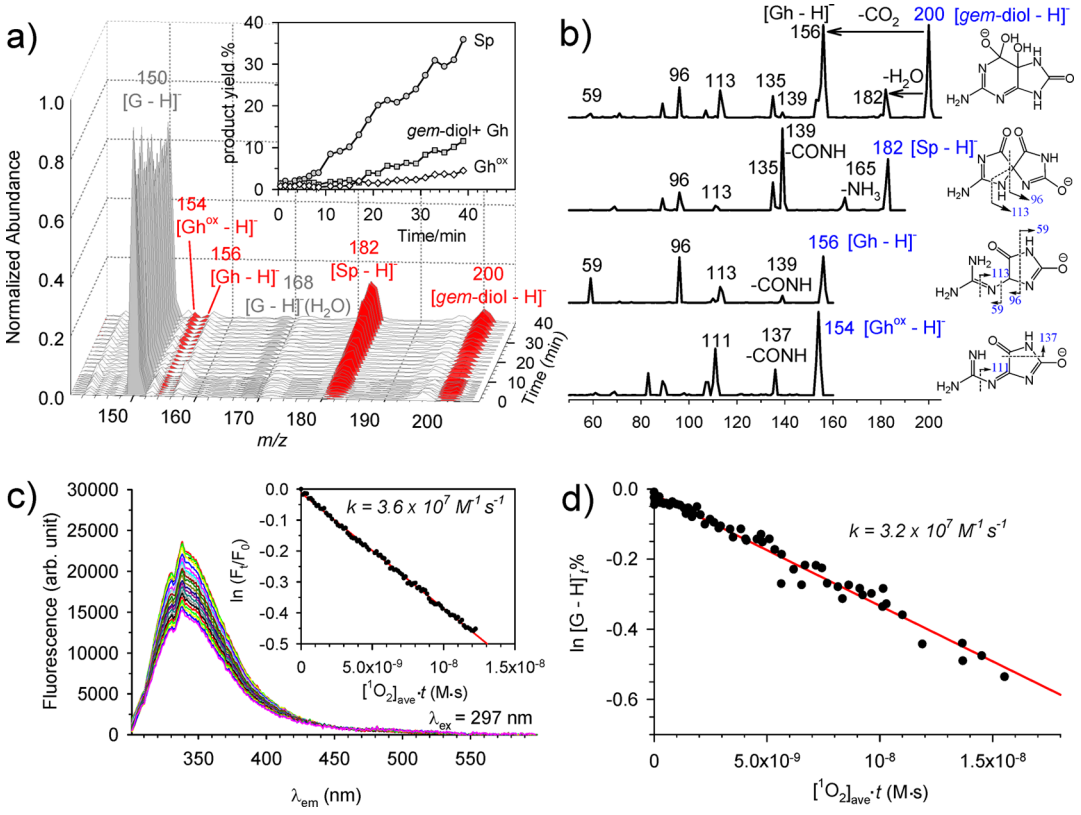

Figure 2. (a) MS measurement for the reaction of guanine + $^1O_2$ at pH 10.0, where the inset shows product yields along the reaction time; (b) CID MS/MS of product ions, where m/z for primary ions is marked in blue; (c) fluorescence spectra and the plot of $\ln(F_t/F_0)$ vs reaction time where F_t and F_0 are the 343 nm emission intensity at different time and time zero; and (d) the plot of $\ln[G - H]^-_t$% vs $[^1O_2]_{av}t$, where $[G - H]^-_t$% is the relative abundance of reactant ion in the MS, and $[^1O_2]_{av}$ is the averaged $[^1O_2]$ over time t.

DOI: 10.1021/acs.jpcb.7b09515
J. Phys. Chem. B 2018, 122, 40−53

m/z 154 to deprotonated Gh^{ox} on the basis of the fact that its fragment ions resemble those of Gh but shift to lower m/z by 2 units. Gh^{ox} was presumed to form in the secondary reaction of OG with $^1O_2$.[14] However, OG itself was not detected in the experiment, most likely owing to its higher reactivity toward $^1O_2$ than guanine. Note that OG was a minor product in the photooxidation of guanine, too.[9,17] We have tentatively attributed m/z 200 to a deprotonated intermediate *gem*-diol,[19,59] which is the precursor for forming $[Gh - H]^-$ (see Scheme 1). The major CID products of [*gem*-diol $- H]^-$ correspond to water elimination at m/z 182 and the formation of $[Gh - H]^-$ at m/z 156 via decarboxylation; the other product ions were most likely generated from the secondary fragmentation of $[Gh - H]^-$. An alternative structure for m/z 200 could be deprotonated 4-carboxyGh, formed by ring-opening of [*gem*-diol $- H]^-$ at N1−C6 with a concurrent proton transfer.[16,48] We were not able to distinguish [*gem*-diol $- H]^-$ and [4-carboxyGh $- H]^-$ in the experiment; however, this would not affect the analysis of reaction kinetics, since [*gem*-diol $- H]^-$ and [4-carboxyGh $- H]^-$ may interconvert and they are the last two intermediates prior to forming $[Gh - H]^-$. Our detection of [*gem*-diol $- H]^-$ and/or [4-carboxyGh $- H]^-$ has supported the formation mechanism for $[Gh - H]^-$ in Scheme 1.[19,56,59]

The inset of Figure 2a plots the changes of individual product yields $(=\frac{\text{product}_i}{\sum_i(\text{reactant} + \text{product}_i)}\%)$ over the reaction time. The intensities of $[Gh - H]^-$ and [*gem*-diol $- H]^-$ were lumped into one group. At the end of the reaction, product branching ratios are $[Sp - H]^- = 0.70$:([*gem*-diol $- H]^-$ + $[Gh - H]^-$) = 0.23:$[Gh^{ox} - H]^- = 0.07$. The domination of $[Sp - H]^-$ under basic conditions is consistent with the previous experimental and theoretical studies.[9,19] The time scale of our experiment was in the range to catch the start of the conversion from [*gem*-diol $- H]^-$/[4-carboxyGh $- H]^-$ to $[Gh - H]^-$. By the end of the reaction, 20% of [*gem*-diol $- H]^-$/[4-carboxyGh $- H]^-$ was converted to $[Gh - H]^-$.

Psciuk and Schlegel have calculated the pK_a values for all oxidation intermediates and products (including OG, OG^{ox}, 5-OHOG, *gem*-diol, 4-carboxyGh, Sp, and Gh) of 9MG.[59] Their results suggest that all intermediates and products are deprotonated at pH 10.0 and thus could be detected by negative ESI MS efficiently. The oxidation of guanine at pH 10.0 was also monitored by the fluorometer (Figure 2c). The fact that the ESI-MS-measured kinetics is consistent with the fluorescence measurement (*vide infra*) has validated our measurements. UV−vis absorption was also measured throughout the reaction, but the overlapping of reactant and product absorption bands prevented the measurement of kinetics.

Reaction PESs. The first four lowest-energy conformers for each of the neutral, protonated, and deprotonated guanine are depicted in Figure S4, along with their relative energies and populations calculated at SMD-ωB97XD/6-31+G(d,p). 9H-keto represents the stable neutral structure in aqueous solution.[60] This structure is 3.9 kJ/mol lower in energy than the 7H-keto tautomer. The two tautomers differ in which of the N9 and N7 positions carries an H atom, and the latter becomes predominant in the gas phase.[21,61] $[G + H]^+\_1$, with N7-protonation of 9H-keto, represents the dominating conformation of protonated guanine with a percentage population of 89%, while $[G - H]^-\_1$ (with N1-deprotonation of 9H-keto, 44% population) is the stable deprotonated structure. We used these global minima conformers as starting structures in reaction coordinate calculations, and calculated all three of the neutral, protonated, and deprotonated systems at the SMD-ωB97XD/aug-cc-pVQZ//SMD-ωB97XD/6-31+G(d,p) levels. Our calculations were focused on the initial $^1O_2$ addition and the formation of end product from late intermediates. For the purpose of comparison, the PESs for different ionization states are plotted together in the two frames of Figure 3, and could be distinguished by different colors. The major PES results are described here.

(1) The early-stage oxidation of guanine in solution is similar to its counterpart system in the gas phase.[21,22] The initial reaction follows reactant + $^1O_2$ → 8-peroxide or 4,8-/5,8-endoperoxide → 8-hydroperoxide → 5-OHOG, as presented in the top frame of Figure 3. Of the different ionization states, the reaction of $[G + H]^+$ bears the highest activation barriers, followed by that of the neutral system. The reaction of $[G - H]^-$ is the most energetically favorable, which agrees with the pH dependence observed in the experiment, i.e., nonoxidative in acidic or neutral solution versus oxidative in basic solution.

(2) Another consequence arising from the different ionization states of guanine concerns the $^1O_2$ addition. A closed-shell calculation for $[G + H]^+ + {}^1O_2$ has led to the formation of a 5,8-endoperoxide $[5,8\text{-OO-G} + H]^+$ via a concerted $^1O_2$ addition with a TS of 4.8 kJ/mol above reactants. However, the same TS connects to an 8-peroxide $[8\text{-OOG} + H]^+$ in the open-shell, broken-symmetry calculation, with the barrier height of 52.5 kJ/mol above reactants and a $\langle \mathbf{S^2} \rangle$ value of 1.01, and $[8\text{-OOG} + H]^+$ then converts to $[5,8\text{-OO-G} + H]^+$ via $TS2^+$ (32.9 kJ/mol). $\langle \mathbf{S^2} \rangle$ is 0.48 at $TS2^+$, and diminishes to zero at $[5,8\text{-OO-G} + H]^+$. $[5,8\text{-OO-G} + H]^+$ subsequently transforms into $[8\text{-H-8-OOHG} + H]^+$ and $[8\text{-OOHG} + H]^+$ via water-assisted proton transfer for which it is less likely to involve very high energy barriers. Alternatively, $[8\text{-OOHG} + H]^+$ may form directly from $[8\text{-OOG} + H]^+$, but with a barrier height calculated to be 64 kJ/mol above $[8\text{-OOG} + H]^+$ in the gas phase.[21] We did not consider the O−O bond opening of $[5,8\text{-OO-G} + H]^+$ in our PES calculations, since that involves a high energy barrier both in the presence[25] and in the absence of water.[21]

Different than the protonated case, both closed- and open-shell calculations of neutral and deprotonated guanine favor the $^1O_2$ addition to C8, resulting in closed-shell 8-OOG (−13.9 kJ/mol) and $[8\text{-OOG} - H]^-$ (−68.0 kJ/mol), respectively. The formation of $[8\text{-OOG} - H]^-$ was confirmed in our direct dynamics trajectory simulations for $[9MG - H]^- + {}^1O_2$ in the gas phase.[22] Stepwise $^1O_2$ addition with the initial formation of an 8-OOG intermediate was also reported in the work of Schlegel et al.[23] and Dumont et al.,[25,26] in which both the isolated entity and the nucleobase within the B-DNA helix have been calculated. 8-OOG and $[8\text{-OOG} - H]^-$ undergo water-assisted proton transfer via TS2 (−6.1 kJ/mol) and $TS2^-$ (−55.0 kJ/mol), producing 8-H-8-OOHG and $[8\text{-H-8-OOHG} - H]^-$, respectively. Downhill, 8-H-8-OOHG/$[8\text{-H-8-OOHG} - H]^-$ may transfer the C8−H atom to N9, producing 8-OOHG/$[8\text{-OOHG} - H]^-$. Finally, an H atom transfer from N1 (or N9) of neutral, protonated, or deprotonated 8-OOHG to the C8-OOH terminal, followed by elimination of a water, would lead to the formation of OG^{ox}, $[OG^{ox} + H]^+$, or $[OG^{ox} - H]^-$. According to the theoretical study on the $^1O_2$ oxidation of guanine by Schlegel et al.,[23] no significant barriers would be expected for these transformations.

Schlegel et al.[23] have suggested the interconversion from 8-OOG to 4,8-OO-G. We have therefore calculated this

DOI: 10.1021/acs.jpcb.7b09515
J. Phys. Chem. B 2018, 122, 40−53

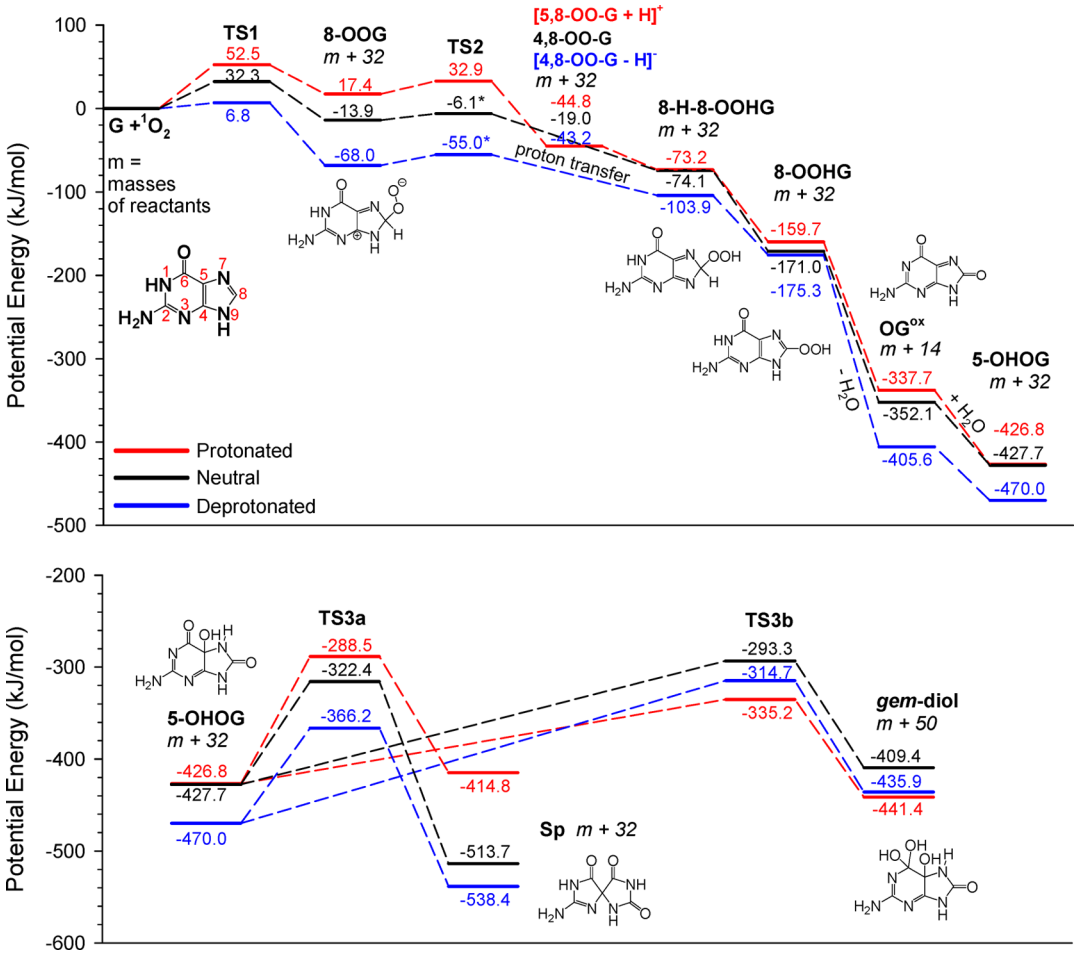

Figure 3. PESs for the reactions of $^1O_2$ with protonated (red), neutral (black), and deprotonated (blue) guanine, with thermal corrections at 298 K. All structures were calculated at SMD-ωB97XD/aug-cc-pVQZ//SMD-ωB97XD/6-31+G(d,p), except for TS3b$^+$ that was calculated at SMD-ωB97XD/aug-cc-pVQZ//PCM-B3LYP/6-31+G(d,p) to avoid convergence failure. Energies of $^1O_2$ and early-stage TSs and intermediates were corrected by approximate spin-projection. Structures of TSs are available in the Supporting Information, and the TS2 energies with asterisks correspond to water-assisted proton transfer.

pathway for both 8-OOG and [8-OOG − H]$^-$. However, the resulting energy barrier is 19.3 kJ/mol above 8-OOG or 34.6 kJ/mol above [8-OOG − H]$^-$, rendering it energetically less favorable, so we did not include this pathway in our PES.

(3) We have calculated the barrier for [OG^{ox} − H]$^-$ + H_2O → [5-OHOG − H]$^-$ in the gas phase, and found that the barrier is 268 kJ/mol below the starting reactants.[21] On the basis of the similar reactions of OG^{ox} in different ionization and reaction conditions, we tend to assume that the pathway leading from OG^{ox} to 5-OHOG should be facile in solution, too.

(4) Finally, the formation of end products from 5-OHOG is pH-dependent. Schlegel et al. have reported the formation pathways of *gem*-diol, Gh, and Sp from 5-OHOG under different conditions using the IEF-PCM/B3LYP/aug-cc-pVTZ//B3LYP/6-31+G(d,p) method.[19] We have adopted their calculated pathways, and refined reaction energetics at the SMD-ωB97XD/aug-cc-pVQZ//SMD-ωB97XD/6-31+G(d,p) levels of theory. The results are summarized in the bottom frame of Figure 3. Protonated [5-OHOG + H]$^+$ (N1-protonated) may convert into [Sp + H]$^+$ via TS3a$^+$ (138.3 kJ/mol above [5-OHOG + H]$^+$) or into [*gem*-diol + H]$^+$ via TS3b$^+$ (91.6 kJ/mol above [5-OHOG + H]$^+$). The latter transformation needs the aid of two water molecules: one is reactive and the other is catalytic as found by Schlegel et al.[19]

Neutral 5-OHOG may transfer a proton from C5-OH to N1, and the resulting tautomer lowers TS3a to 29.2 kJ/mol below TS3b, favoring the formation of Sp over *gem*-diol. Similar to 5-OHOG, [5-OHOG − H]$^-$ (deprotonated at N9) adopts an intramolecular proton transfer from C5-OH to N9 to enhance the product channel of [Sp − H]$^-$; i.e., TS3a$^-$ is 51.5 kJ/mol lower than TS3b$^-$. Our calculations with the different DFT method have reproduced the pH-dependent formation of Sp versus Gh predicted by Schlegel et al. Such theoretical predications agree with our experimental product branching ratio of [Sp − H]$^-$/[Gh − H]$^-$. [*gem*-diol − H]$^-$ would ultimately undergo ring rupture to form [4-carboxyGh − H]$^-$, followed by decarboxylation to [Gh − H]$^-$.[19] In our experiment, no more than 20% of [*gem*-diol − H]$^-$ was converted into [Gh − H]$^-$ within 40 min. Apparently our reaction system was trapped within the potential well of *gem*-diol for some time before it crossed over the exit-channel barriers.

Kinetics. Guided by the PES analysis, the oxidation of guanine in basic solution consists of the following steps:

$$[G - H]^- + {}^1O_2 \underset{k_{-1}^-}{\overset{k_1^-}{\rightleftharpoons}} [8\text{-OOG} - H]^-$$

$$\Delta H_{r1}^- = -68.0 \text{ kJ/mol and } E_{a1}^- = 6.8 \text{ kJ/mol} \quad \text{(S1)}$$

DOI: 10.1021/acs.jpcb.7b09515
J. Phys. Chem. B 2018, 122, 40−53

$$[\text{8-OOG} - \text{H}]^- \rightarrow [\text{8-H-8-OOHG} - \text{H}]^-$$
$$\Delta H_{r2}^- = -36.0\ \text{kJ/mol} \quad \text{(S2)}$$

$$[\text{8-H-8-OOHG} - \text{H}]^- \rightarrow [\text{8-OOHG} - \text{H}]^-$$
$$\Delta H_{r3}^- = -71.4\ \text{kJ/mol} \quad \text{(S3)}$$

$$[\text{8-OOHG} - \text{H}]^- \rightarrow [\text{OG}^{ox} - \text{H}]^- + \text{H}_2\text{O}$$
$$\Delta H_{r4}^- = -230.2\ \text{kJ/mol} \quad \text{(S4)}$$

$$[\text{OG}^{ox} - \text{H}]^- + \text{H}_2\text{O} \rightarrow [\text{5-OHOG} - \text{H}]^-$$
$$\Delta H_{r5}^- = -64.4\ \text{kJ/mol} \quad \text{(S5)}$$

$$[\text{5-OHOG} - \text{H}]^- \rightarrow [\text{Sp} - \text{H}]^-$$
$$\Delta H_{r6a}^- = -68.4\ \text{kJ/mol} \quad \text{(S6a)}$$

$$[\text{5-OHOG} - \text{H}]^- + \text{H}_2\text{O} \rightarrow [\textit{gem}\text{-diol} - \text{H}]^-$$
$$\Delta H_{r6b}^- = 34.1\ \text{kJ/mol} \quad \text{(S6b)}$$

Step S1 is an elementary reaction, and its reverse step could be discounted since the reverse barrier is 68.0 kJ/mol higher than the forward one. Steps S2 and S3 are water-assisted proton transfer, and S4 and S5 are the conversions from $[\text{8-OOHG} - \text{H}]^-$ to $[\text{5-OHOG} - \text{H}]^-$. None of these steps involve barriers above the starting reactants; therefore, they are expected to happen readily. $[\text{5-OHOG} - \text{H}]^-$ is the last intermediate before the formation of end products via steps S6a and S6b. This was detected only in the low-temperature oxidation of a modified guanosine, and quickly rearranged to Sp upon warming to room temperature.[13,62] Thus, it is reasonable to assume that S6a and/or S6b are also facile. It follows that the $^1O_2$ oxidation of $[\text{G} - \text{H}]^-$ may be treated as a first-order consecutive reaction,[63,64] of which step S1 is rate-limiting. The overall kinetics could be described by eq 2 and its integrated form eq 3:

$$-\frac{\text{d}[[\text{G} - \text{H}]^-]}{\text{d}t} = k_1^-[[\text{G} - \text{H}]^-][^1\text{O}_2] \quad (2)$$

$$\ln[\text{G} - \text{H}]^-_t\% = \ln\{([[\text{G} - \text{H}]^-]_t)/([[\text{G} - \text{H}]^-]_t + [[\text{Sp} - \text{H}]^-]_t + [[\textit{gem}\text{-diol} - \text{H}]^-]_t + [[\text{Gh}^{ox} - \text{H}]^-]_t)\} = -k_1^-[^1\text{O}_2]_{av}t \quad (3)$$

where $[[\text{G} - \text{H}]^-]_t$, $[[\text{Sp} - \text{H}]^-]_t$, $[[\textit{gem}\text{-diol} - \text{H}]^-]_t$, and $[[\text{Gh}^{ox} - \text{H}]^-]_t$ are the concentrations of the reactant and the products, and $[\text{G} - \text{H}]^-_t\%$ is the relative abundance of the reactant ion at reaction time t. $[^1O_2]_{av}$ was averaged over the integration period from 0 to t. The concentration of $[\text{Gh} - \text{H}]^-$ was lumped into that of $[\textit{gem}\text{-diol} - \text{H}]^-$. As shown in Figure 2d, the plot of $\ln[\text{G} - \text{H}]^-_t\%$ versus $[^1O_2]_{av}t$ fits into a linear relationship, from which a value of $3.2 \times 10^7\ \text{M}^{-1}\ \text{s}^{-1}$ was extracted for k_1^-. Rate constants of forming $[\text{Sp} - \text{H}]^-$ and $[\textit{gem}\text{-diol} - \text{H}]^-$ may be estimated from product branching ratios: that is, $2.2 \times 10^7\ \text{M}^{-1}\ \text{s}^{-1}$ for $[\text{Sp} - \text{H}]^-$ and $0.7 \times 10^7\ \text{M}^{-1}\ \text{s}^{-1}$ for $[\textit{gem}\text{-diol} - \text{H}]^-$. The interconversion between $[\text{Gh} - \text{H}]^-$ and $[\text{Sp} - \text{H}]^-$ would happen on time scales from days to a week,[24] and thus was not considered here.

The kinetics for $[\text{G} - \text{H}]^- + {}^1\text{O}_2$ was also analyzed on the basis of the changes of the $[\text{G} - \text{H}]^-$ emission intensity over the reaction time, as shown in the inset of Figure 2c. The fluorescence-measured k_1^- is $3.6 \times 10^7\ \text{M}^{-1}\ \text{s}^{-1}$. On the basis of the cross-checking between MS and fluorescence measurements, the relative uncertainty for the k_1^- measurement is within ±10%. Since guanine is oxidizable only in its deprotonated form, the rate constant measured at pH 10.0 represents the actual rate constant for $[\text{G} - \text{H}]^-$.

3.2. $^1O_2$ Oxidation of 9MG. 9MG was found to be much more reactive than guanine. We have observed the oxidation of 9MG at all different pH values, albeit the reaction was still slow under acidic and neutral conditions. At pH = 3.0, the oxidation product was observed only at m/z 172 in the mass spectra of Figure 4, which could be attributed to $[\text{9MGh} + \text{H}]^+$. Different than the reaction of $[\text{G} - \text{H}]^- + {}^1\text{O}_2$ where both $[\text{Gh} - \text{H}]^-$ and its precedent intermediate $[\textit{gem}\text{-diol} - \text{H}]^-$ were detected (Figure 2a), $[\textit{gem}\text{-9Mdiol} + \text{H}]^+$ (m/z 216) was missing in Figure 4, indicating that the conversion of $[\textit{gem}\text{-9Mdiol} + \text{H}]^+$ becomes much faster. Such a pH-dependent difference is due to the fact that the activation barrier leading from *gem*-diol to Gh decreases under acidic conditions. According to the IEF-PCM/B3LYP/aug-cc-pVTZ//B3LYP/6-31+G(d,p) calculation,[19] the exit barrier to $[\text{Gh} + \text{H}]^+$ is only half of that to neutral Gh.

The major oxidation products of neutral 9MG include 9MGh^{ox} (m/z 170), 9MGh (m/z 172), 9MSp (m/z 198), and *gem*-9Mdiol (m/z 216), all of which were detected in protonated forms in positive ESI MS (Figure 5a). CID mass spectra of these product ions were reported in Figure 5b. Their fragmentation features are consistent with the positive ESI MS/MS of free Sp and Gh reported by the Burrows group,[9,57,58] except for the fragments at $[m - 9]$ which may come from secondary reactions during collisions of precursor ions. The product branching ratio of 9MSp versus (*gem*-9Mdiol + 9MGh) is 1.4:1 at the end of the measurement.

There is a minor product observed at m/z 201 for neutral 9MG. We were not able to determine its structure in the present experiment. However, it is worth mentioning that the CID pattern of m/z 201 resembles that of 5-carboxamido-5-formamido-2-iminohydantoin (2Ih).[65] The latter was reported in the reactions of guanine and guanosine with $^\bullet\text{OH}$[65,66] and dimethyldioxirane.[67]

Similar to guanine, 9MG underwent profound oxidation at pH 10.0. The oxidation products of $[\text{9MG} - \text{H}]^-$ and their CID results, presented in Figure 6a,b, are similar to their guanine analogues with the only difference being that deprotonated 8-oxo-7,8-dihydro-9-methylguanine ($[\text{9MOG} - \text{H}]^-$) was detected in the oxidation of $[\text{9MG} - \text{H}]^-$. As indicated above, OG is the major oxidation product of the guanine nucleobase within DNA.[13,68,69] CID of $[\text{9MOG} - \text{H}]^-$ was found to follow dissociation pathways similar to those of $[\text{OG} + \text{H}]^+$.[70] Final product branching ratio is $[\text{9MSp} - \text{H}]^-$:($[\textit{gem}\text{-9Mdiol} - \text{H}]^-$ + $[\text{9MGh} - \text{H}]^-$):($[\text{9MGh}^{ox} - \text{H}]^-$ + $[\text{9MOG} - \text{H}]^-$) = 72:9:19. A similar Sp population was reported in the photooxidation products of guanosine at pH 8.6.[9,17] Compared to that for $[\text{G} - \text{H}]^-$, 9-methyl substitution of guanine increases the ratio of $[\text{9MSp} - \text{H}]^-$/($[\textit{gem}\text{-9Mdiol} - \text{H}]^-$ + $[\text{9MGh} - \text{H}]^-$) by a factor of 2.5.

9MG showed fluorescence only at pH 3.0 (λ_{em} = 369 nm when excited at 290 nm). However, the change of the emission intensity was insignificant throughout the reaction, and the signal-to-noise ratio was insufficient for kinetic analysis. UV−vis spectroscopy was not able to detect absorbance changes during

DOI: 10.1021/acs.jpcb.7b09515
J. Phys. Chem. B 2018, 122, 40−53

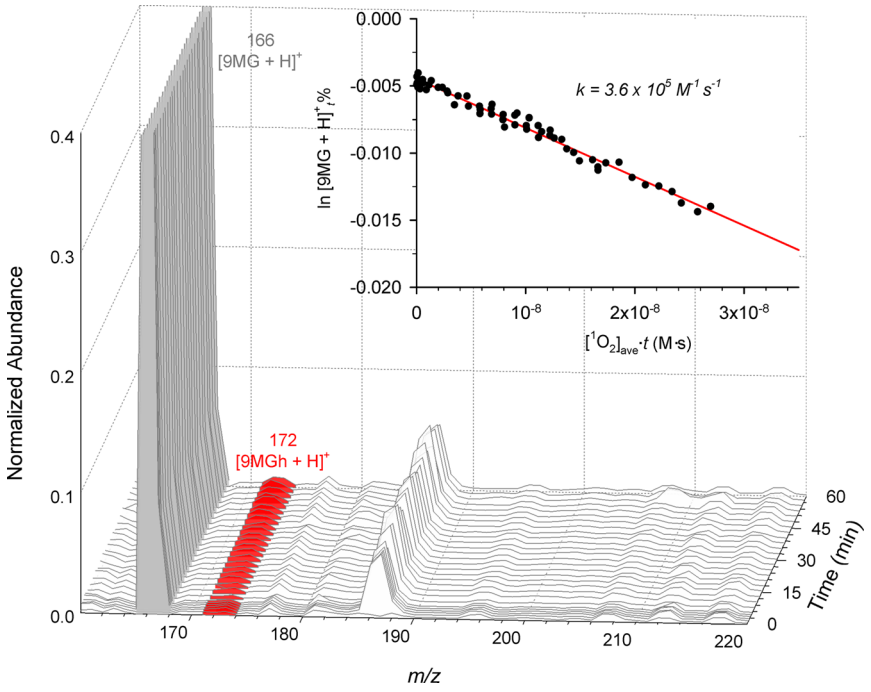

Figure 4. MS measurement for the reaction of 9MG + $^1O_2$ at pH 3.0. For a clear presentation of product signals, the scale for ion abundance was plotted only up to 0.4. Inset shows the plot of ln$[9MG + H]^+_t$% vs $[^1O_2]_{av}t$, where $[9MG + H]^+_t$% is the relative abundance of reactant ion, and $[^1O_2]_{av}$ is the averaged $[^1O_2]$ over time *t*.

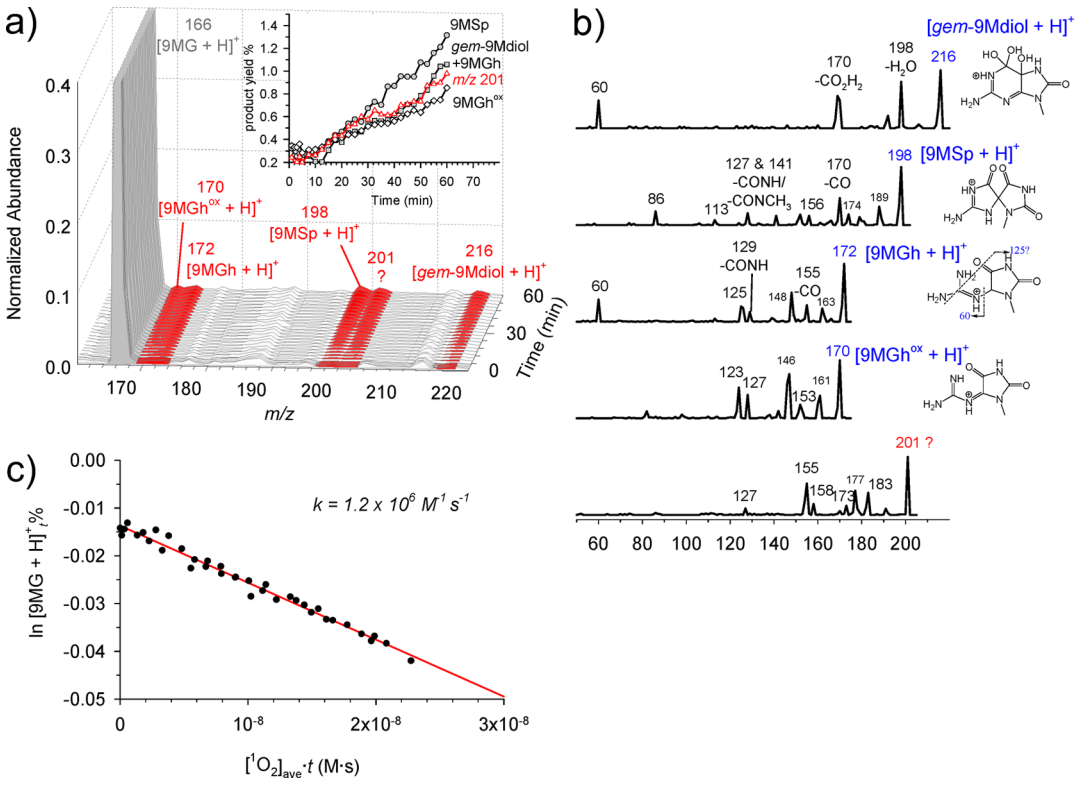

Figure 5. (a) MS measurement for the reaction of 9MG + $^1O_2$ at pH 7.0. For a clear presentation of product signals, the scale for ion abundance was plotted only up to 0.4. The inset shows product yields along the reaction time. (b) CID MS/MS of product ions, where *m*/*z* for primary ions is marked in blue (or red). (c) Plot of ln$[9MG + H]^+_t$% vs $[^1O_2]_{av}t$, where $[9MG + H]^+_t$% is the relative abundance of reactant ion in the MS, and $[^1O_2]_{av}$ is the averaged $[^1O_2]$ over time *t*.

the reaction of 9MG at pH 3.0 and 7.0, either, but it revealed dramatic bleaching of 9MG absorbance at pH 10.0 as illustrated in Figure 6c. The bleaching of the 9MG absorption at 241−288 nm was accompanied by the increasing product absorption in the ranges 220−241 and 288−450 nm, with isosbestic points found at 241 and 288 nm.

DOI: 10.1021/acs.jpcb.7b09515
J. Phys. Chem. B 2018, 122, 40−53

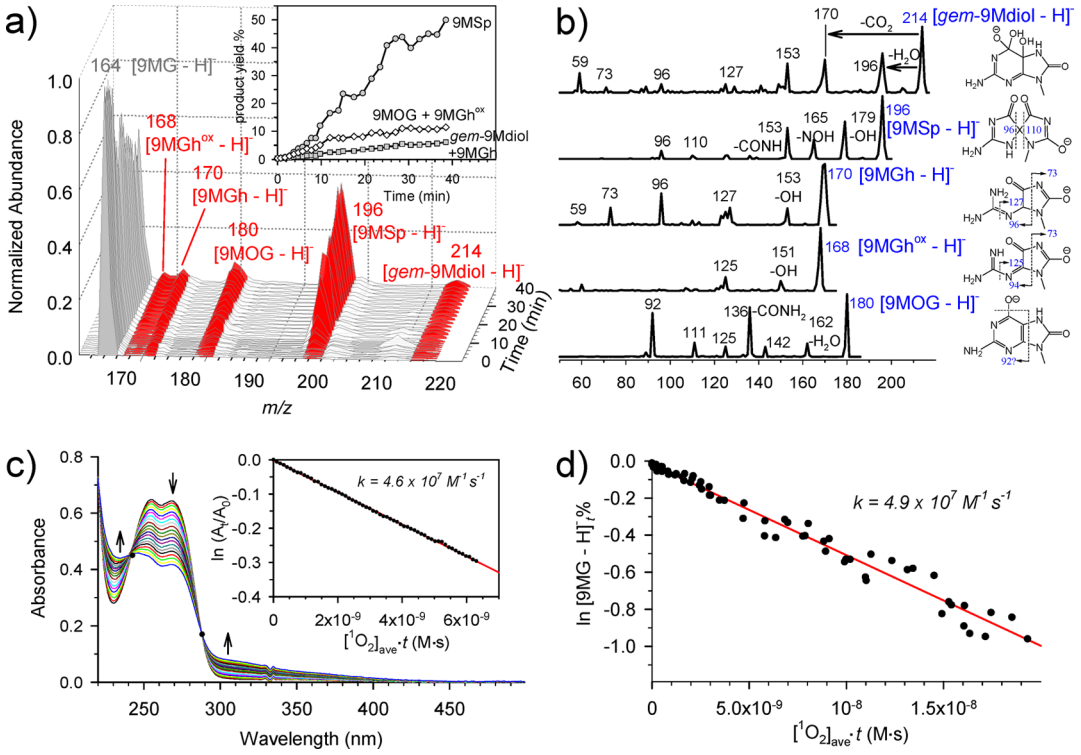

Figure 6. (a) MS measurement for the reaction of 9MG + $^1O_2$ at pH 10.0, where the inset shows product yields along the reaction time. (b) CID MS/MS of product ions, where m/z for primary ions is marked in blue. (c) UV−vis absorption spectra and the plot of $\ln(A_t/A_0)$ vs reaction time, where A_t and A_0 are the absorbance at 268 nm at different times and time zero. (d) Plot of $\ln[9MG - H]^-_t\%$ vs $[^1O_2]_{av}t$, where $[9MG - H]^-_t\%$ is the relative abundance of reactant ion in MS, and $[^1O_2]_{av}$ is the averaged $[^1O_2]$ over time t.

Reaction PESs. The SMD-ωB97XD/6-31+G(d,p)-calculated conformers for neutral, protonated, and deprotonated 9MG are given in Figure S4. All minimum-energy conformers are overwhelmingly predominant (nearly 100%) in the respective series, and resemble their guanine counterparts in structures except that N9 is capped with a methyl group. As a result, the PES profiles for 9MG + $^1O_2$ in Figure 7 are similar to those for G + $^1O_2$. Here only the differences and their kinetic consequences are addressed: (1) Compared to guanine, the rate-limiting barriers for 9MG (i.e., TS1 for $^1O_2$ addition) are lower by 3−7 kJ/mol. As a result, 9MG becomes more reactive. (2) As described in section 3.1, 8-peroxides of neutral and deprotonated G may undergo successive water-assisted proton transfer from N9 to the peroxide terminal. This pathway becomes forbidden with N9-methylation. Instead, 8-OO9MG converts to 4,8-OO-9MG via TS2, and then 8-H-8-OOH9MG and 8-OOH9MG via protonation and deprotonation, and $[8\text{-OO9MG} - H]^-$ converts to $[8\text{-OOH9MG} - H]^-$ without the intermediacy of $[8\text{-H-8-OOH9MG} - H]^-$. (3) For $[G - H]^- + {}^1O_2$, the barrier of TS3a$^-$ leading to $[Sp - H]^-$ is 103.8 kJ/mol above $[5\text{-OHOG} - H]^-$, and that of TS3b$^-$ to $[gem\text{-diol} - H]^-$ is 155.3 kJ/mol. For the $[9MG - H]^-$ system, TS3a$^-$ and TS3b$^-$ become 70.6 and 134.5 kJ/mol above $[5\text{-OH9MOG} - H]^-$, respectively. The barrier to $[9MSp - H]^-$ reduces remarkably, making the product branching to $[9MSp - H]^-$ more favorable with respect to $[gem\text{-9Mdiol} - H]^-$.

Kinetics. The PES for $[9MG + H]^+ + {}^1O_2$ indicates two barriers TS1$^+$ and TS2$^+$ above the reactants, which correspond to the following two consecutive elementary steps:

$$[9MG + H]^+ + {}^1O_2 \underset{k_{-1}^+}{\overset{k_1^+}{\rightleftharpoons}} [8\text{-OO9MG} + H]^+ \quad (4)$$

$$[8\text{-OO9MG} + H]^+ \overset{k_2^+}{\rightarrow} [5,8\text{-OO-9MG} + H]^+ \quad (5)$$

We have estimated from relative barrier heights that the rate constant for the reverse direction of reaction 4 is 2 orders of magnitude lower than that of reaction 5. Thus, the oxidation kinetics for $[9MG + H]^+$ could be approximated as

$$-\frac{d[[9MG + H]^+]}{dt} = k_1^+[[9MG + H]^+][^1O_2] \quad (6)$$

and

$$\ln [9MG + H]^+_t\% = -k_1^+[^1O_2]_{av}t \quad (7)$$

Similar kinetic equations may be obtained for the oxidation of neutral and deprotonated 9MG:

$$\ln 9MG_t\% = -k_1[^1O_2]_{av}t \quad (8)$$

$$\ln [9MG - H]^-_t\% = -k_1^-[^1O_2]_{av}t \quad (9)$$

Equations 7−9 are plotted in Figures 4−6, using both MS and UV−vis analysis results. Measured rate constants are 3.6 × 10^5 M^{-1} s^{-1} at pH 3.0, 1.2 × 10^6 M^{-1} s^{-1} at pH 7.0, and 4.6−4.9 × 10^7 M^{-1} s^{-1} at pH 10. Note that on the basis of 9MG pK_a values (pK_1 = 3.11 and pK_2 = 9.56),[30] the 9MG solution is composed of $[9MG + H]^+$ (56%) + 9MG (44%) at pH 3.0, 9MG (100%) at pH 7.0, and 9MG (27%) + $[9MG - H]^-$ (73%) at pH 10.0. Considering that the rate constant measured at pH 3.0 is only 30% of that at pH 7 and that the pH 3 solution contains 44% of neutral 9MG, it could be inferred that the oxidation observed at pH 3 was actually contributed from the reaction of neutral 9MG (note neutral products were protonated in the positive ESI MS). It follows that the reaction

DOI: 10.1021/acs.jpcb.7b09515
J. Phys. Chem. B 2018, 122, 40−53

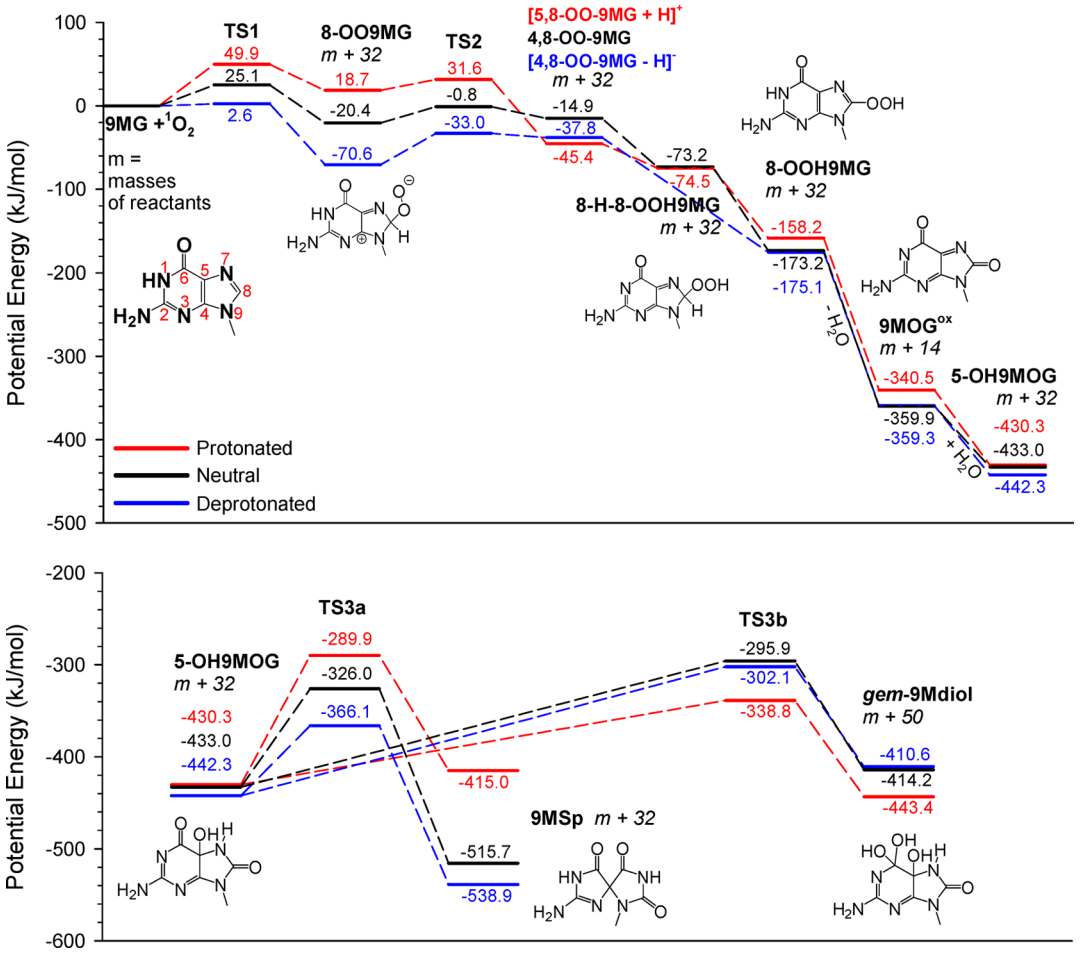

Figure 7. PESs for the reactions of $^1O_2$ with protonated (red), neutral (black), and deprotonated (blue) 9MG, with thermal corrections at 298 K. All structures were calculated at SMD-ωB97XD/aug-cc-pVQZ//SMD-ωB97XD/6-31+G(d,p), except for TS3b$^+$ that was calculated at SMD-ωB97XD/aug-cc-pVQZ//PCM-B3LYP/6-31+G(d,p) to avoid convergence failure. Energies of $^1O_2$ and early-stage TSs and intermediates were corrected by approximate spin-projection. Structures of TSs are available in the Supporting Information.

Table 1. Experimental Reaction Rate Constants and Product Branching Ratios

	rate constant (M^{-1} s^{-1})[a]		product branching ratio[b]	
ionization state	G	9MG	G	9MG
protonated				
neutral		1.2×10^6		9MSp:(*gem*-9Mdiol +9MGh):9MGh^{ox} = 0.45:0.33:0.22
deprotonated	3.2×10^7	4.9×10^7	Sp:(*gem*-diol + Gh):Gh^{ox} = 0.70:0.23:0.07	9MSp:(*gem*-9Mdiol + 9MGh):(9MOG + 9MGh^{ox}) = 0.72:0.09:0.19
	3.6×10^7*	4.6×10^7*		

[a]Values marked with asterisks were measured by spectroscopy, and the others were measured by ESI MS. [b]Measured at the end of reactions.

of $[9MG + H]^+ + {}^1O_2$ is negligible. Population-corrected rate constants and product branching ratios are summarized in Table 1.

We have calculated the rate constants for the initial $^1O_2$ addition using thermodynamic transition state theory (TST):[71]

$$k(T) = \sigma \frac{k_B T}{h} e^{-\Delta G^{\circ,\ddagger}(T)/k_B T} \quad (10)$$

where σ is the reaction path degeneracy, k_B is Boltzmann's constant, T is the reaction temperature, h is Planck's constant, and $\Delta G^{\circ,\ddagger}(T)$ represents the standard Gibbs free energy of activation. The volume change at the TS was set to zero by using the solution-phase approximation.[63] All of the energetics and frequencies were extracted from open-shell approximately spin-projected DFT calculations. Results are summarized in Table 2. It turns out that the TST theory was able to predict the pH dependence for the oxidation of guanine and 9MG. However, the calculated rate constants based on SMD-ωB97XD/aug-cc-pVQZ energies are lower than the experimental values. The large deviation between the absolute values of experimental and DFT-calculated k_1 may be attributed to the mixing of the inaccuracy in the DFT calculations of multireferential characters and the experimental uncertainty arising from the low reaction efficiency (<0.01%).

3.3. Differences between Gas- and Solution-Phase Oxidation. Our previous gas-phase work has examined the reactivities of isolated guanine and 9MG toward $^1O_2$, separated from solvent and counterion effects. Gas-phase findings have provided a basis for understanding their intrinsic reactivities and early-stage reaction dynamics. The combination with the

DOI: 10.1021/acs.jpcb.7b09515
J. Phys. Chem. B 2018, 122, 40−53

Table 2. DFT-Calculated Activation Barriers and TST-Predicted Rate Constants

	SMD-ωB97XD/aug-cc-pVQZ				SMD-ωB97XD/6-31+G(d,p)			
	TS1 (kJ/mol)		k_1 (M^{-1} s^{-1})		TS1 (kJ/mol)		k_1 (M^{-1} s^{-1})	
ionization state	G	9MG	G	9MG	G	9MG	G	9MG
protonated	52.5	49.9	1.6×10^{-4}	2.6×10^{-4}	42.4	39.1	8.8×10^{-3}	1.9×10^{-2}
neutral	32.3	25.1	0.4	1.3	17.3	9.9	1.4×10^{2}	5.5×10^{2}
deprotonated	6.8	2.6	4.8×10^{4}	3.6×10^{5}	−8.4	−12.8	2.1×10^{7}	1.7×10^{8}

parallel solution-phase study of the same systems leads to a panoramic view and improves our understanding of guanine oxidation chemistry.

Both in the gas phase and in solution, the oxidation of guanine and 9MG is initiated by O_2 adducts formed between $^1O_2$ and the imidazole ring, and the structures of adducts may vary with the reactant ionization states. A fact that has complicated the comparison of gas- and solution-phase guanine reactions is that guanine comprises 24% of 9H-keto and 69% of 7H-keto in the gas phase, whereas respective populations become 81% and 19% in aqueous solution. Note that, of the two tautomers, the 7H-keto tautomer is not biochemically relevant. Upon deprotonation, the dominating structure corresponds to N1-deprotonated 7H-keto (i.e., $[G - H]^-$_2 in Figure S4) in the gas phase versus N1-deprotonated 9H-keto (i.e., $[G - H]^-$_1 in Figure S4) in solution. This affects the addition mechanism: gas-phase $[G - H]^-$ forms a 5,8-endoperoxide via a concerted $^1O_2$ addition, whereas solution-phase $[G - H]^-$ forms an 8-peroxide which may convert to a 4,8-endoperoxide via a stepwise addition. Different deprotonated structures also affect the way in which the 9-methyl substitution modulates reactions. In solution, $[9MG - H]^-$ and $[G - H]^-$ adopt similar structures, and the reaction efficiency of $[9MG - H]^-$ is 40% higher than that of $[G - H]^-$. In contrast, in the gas phase, the 9-methyl substitution suppresses the oxidizability of $[G - H]^-$ by ∼40% due to the N7H−N9H tautomerization.[21,22]

Another difference between gas- and solution-phase oxidation concerns the ionization state or pH dependence. Protonated and deprotonated guanine (and 9MG) have nearly the same reaction efficiencies of forming endoperoxide or peroxide in the gas phase (2.5% for guanine and 1.5% for 9MG, measured at E_{col} = 0.1 eV).[21,22] On the contrary, the solution experiment revealed contrasting reactivities at different pH values. The oxidation of guanine/9MG is the most remarkable under basic conditions. The reactions become minor under neutral solutions, and shut down completely under acidic conditions. Similar pH dependence has been observed in the $^1O_2$ oxidation of histidine.[35] In the latter case, the oxidation of protonated histidine is mediated by the 2,5-endoperoxide and 5-hydroperoxide of the imidazole ring, which convert to the stable imidazolone end product in solution, whereas the oxidation of deprotonated histidine involves the formation of the 2,4-endoperoxide and 2-hydroperoxide of imidazole, which ultimately evolve to 6α-hydroxy-2-oxo-octahydro-pyrrolo[2,3-*d*]-imidazole-5-carboxylate or cross-link with another histidine. A common feature for the oxidation of guanine and histidine is that both reactions are initiated by the $^1O_2$ addition to an imidazole ring. A protonated imidazole ring would generally lower the π-electron density and its attraction to $^1O_2$, and increase the decomposition of nascent endoperoxide back to reactants.

4. CONCLUSIONS

We have studied the reaction kinetics of $^1O_2$ with guanine and 9MG in aqueous solution of pH 3.0, 7.0, and 10.0, using a newly updated online reaction monitoring system consisting of an ESI tandem mass spectrometer and UV−vis absorption and fluorescence spectrophotometers. All of the reactions were found to obey a first-order rate law. On the basis of the populations of different ionization states in the reaction solutions, the rate constants were determined to be 3.2−3.6 × 10^7 M^{-1} s^{-1} for $[G - H]^-$ + $^1O_2$, 1.2 × 10^6 M^{-1} s^{-1} for 9MG + $^1O_2$, and 4.6−4.9 × 10^7 M^{-1} s^{-1} for $[9MG - H]^-$ + $^1O_2$. No oxidation was detected for G, $[G + H]^+$, or $[9MG + H]^+$. The kinetic results have revealed strong pH dependence of guanine oxidation and the influence of the 9-methyl substitution. Product structures and branching ratios were determined by MS and MS/MS, and their formation mechanisms were elucidated at the SMD-ωB97XD/aug-cc-pVQZ//SMD-ωB97XD/6-31+G(d,p) level of theory. The oxidation of 9MG under neutral conditions produced 9MSp, *gem*-9Mdiol, 9MGh, and $9MGh^{ox}$. Similar products were formed in the oxidation of guanine and 9MG in basic solutions, and 9MSp became predominant under these conditions. In addition, the first experimental detection of the *gem*-diol intermediates has supported the formation mechanism of Gh.

■ ASSOCIATED CONTENT

Supporting Information

The Supporting Information is available free of charge on the ACS Publications website at DOI: 10.1021/acs.jpcb.7b09515.

Calibration of $[^1O_2]$ in solution; ESI MS spectra for guanine + $^1O_2$ at pH 3.0 and 7.0; tautomers of protonated, neutral, and deprotonated guanine and 9MG and their Cartesian coordinates; Cartesian coordinates of all structures in Figures 3 and 7; and the GaussView images of TSs (PDF)

■ AUTHOR INFORMATION

Corresponding Author

*E-mail: jianbo.liu@qc.cuny.edu. Phone: 1-718-997-3271.

ORCID

Jianbo Liu: 0000-0001-9577-3740

Notes

The authors declare no competing financial interest.

■ ACKNOWLEDGMENTS

This work was supported by the National Science Foundation (Grant CHE 1464171), PSC-CUNY Research Award, and Queens College Research Enhancement Award. W.L. and Y.S. acknowledge a CUNY Doctoral Student Research Grant. The authors thank B. Thapa (the Schlegel group at Wayne State University) for help with spin-projection calculations.

■ REFERENCES

(1) Marnett, L. J.; Burcham, P. C. Endogenous DNA Adducts: Potential and Paradox. *Chem. Res. Toxicol.* **1993**, *6*, 771−85.

DOI: 10.1021/acs.jpcb.7b09515
J. Phys. Chem. B 2018, 122, 40−53

(2) Armitage, B. Photocleavage of Nucleic Acids. *Chem. Rev.* **1998**, *98*, 1171−1200.
(3) Burrows, C. J.; Muller, J. G. Oxidative Nucleobase Modifications Leading to Strand Scission. *Chem. Rev.* **1998**, *98*, 1109−1151.
(4) *Singlet Oxygen: Applications in Biosciences and Nanosciences*; Nonell, S., Flors, C., Eds.; RSC, 2016; Vol. *1*.
(5) Sheu, C.; Foote, C. S. Endoperoxide Formation in a Guanosine Derivative. *J. Am. Chem. Soc.* **1993**, *115*, 10446−10447.
(6) Ravanat, J.-L.; Di Mascio, P.; Martinez, G. R.; Medeiros, M. H. G.; Cadet, J. Singlet Oxygen Induces Oxidation of Cellular DNA. *J. Biol. Chem.* **2000**, *275*, 40601−40604.
(7) Niles, J. C.; Wishnok, J. S.; Tannenbaum, S. R. Spiroiminodihydantoin Is the Major Product of the 8-Oxo-7,8-Dihydroguanosine Reaction with Peroxynitrite in the Presence of Thiols and Guanosine Photooxidation by Methylene Blue. *Org. Lett.* **2001**, *3*, 963−966.
(8) Kang, P.; Foote, C. S. Formation of Transient Intermediates in Low-Temperature Photosensitized Oxidation of an 8-^{13}C-Guanosine Derivative. *J. Am. Chem. Soc.* **2002**, *124*, 4865−4873.
(9) Ye, Y.; Muller, J. G.; Luo, W.; Mayne, C. L.; Shallop, A. J.; Jones, R. A.; Burrows, C. J. Formation of ^{13}C-, ^{15}N-, and ^{18}O-Labeled Guanidinohydantoin from Guanosine Oxidation with Singlet Oxygen. Implications for Structure and Mechanism. *J. Am. Chem. Soc.* **2003**, *125*, 13926−13927.
(10) McCallum, J. E. B.; Kuniyoshi, C. Y.; Foote, C. S. Characterization of 5-Hydroxy-8-Oxo-7,8-Dihydroguanosine in the Photosensitized Oxidation of 8-Oxo-7,8-Dihydroguanosine and Its Rearrangement to Spiroiminodihydantoin. *J. Am. Chem. Soc.* **2004**, *126*, 16777−16782.
(11) Iesce, M. R.; Cermola, F.; Temussi, F. Photooxygenation of Heterocycles. *Curr. Org. Chem.* **2005**, *9*, 109−139.
(12) Ravanat, J.-L.; Martinez, G. R.; Medeiros, M. H. G.; Di Mascio, P.; Cadet, J. Singlet Oxygen Oxidation of 2′-Deoxyguanosine. Formation and Mechanistic Insights. *Tetrahedron* **2006**, *62*, 10709−10715.
(13) Cadet, J.; Ravanat, J.-L.; Martinez, G. R.; Medeiros, M. H. G.; Di Mascio, P. Singlet Oxygen Oxidation of Isolated and Cellular DNA: Product Formation and Mechanistic Insights. *Photochem. Photobiol.* **2006**, *82*, 1219−1225.
(14) Neeley, W. L.; Essigmann, J. M. Mechanisms of Formation, Genotoxicity, and Mutation of Guanine Oxidation Products. *Chem. Res. Toxicol.* **2006**, *19*, 491−505.
(15) Cadet, J.; Douki, T.; Ravanat, J.-L. Oxidatively Generated Damage to the Guanine Moiety of DNA: Mechanistic Aspects and Formation in Cells. *Acc. Chem. Res.* **2008**, *41*, 1075−1083.
(16) Cadet, J.; Douki, T.; Ravanat, J.-L. Oxidatively Generated Base Damage to Cellular DNA. *Free Radical Biol. Med.* **2010**, *49*, 9−21.
(17) Fleming, A. M.; Burrows, C. J. Formation and Processing of DNA Damage Substrates for the nNEIL Enzymes. *Free Radical Biol. Med.* **2017**, *107*, 35−52.
(18) Ravanat, J.-L.; Martinez, G. R.; Medeiros, M. H. G.; Di Mascio, P.; Cadet, J. Mechanistic Aspects of the Oxidation of DNA Constituents Mediated by Singlet Molecular Oxygen. *Arch. Biochem. Biophys.* **2004**, *423*, 23−30.
(19) Munk, B. H.; Burrows, C. J.; Schlegel, H. B. An Exploration of Mechanisms for the Transformation of 8-Oxoguanine to Guanidinohydantoin and Spiroiminodihydantoin by Density Functional Theory. *J. Am. Chem. Soc.* **2008**, *130*, 5245−5256.
(20) Sheu, C.; Kang, P.; Khan, S.; Foote, C. S. Low-Temperature Photosensitized Oxidation of a Guanosine Derivative and Formation of an Imidazole Ring-Opened Product. *J. Am. Chem. Soc.* **2002**, *124*, 3905−3913.
(21) Lu, W.; Liu, J. Capturing Transient Endoperoxide in the Singlet Oxygen Oxidation of Guanine. *Chem. - Eur. J.* **2016**, *22*, 3127−3138.
(22) Lu, W.; Teng, H.; Liu, J. How Protonation and Deprotonation of 9-Methylguanine Alter Its Singlet O_2 Addition Path: About the Initial Stage of Guanine Nucleoside Oxidation. *Phys. Chem. Chem. Phys.* **2016**, *18*, 15223−15234.
(23) Thapa, B.; Munk, B. H.; Burrows, C. J.; Schlegel, H. B. Computational Study of Oxidation of Guanine by Singlet Oxygen ($^1\Delta_g$) and Formation of Guanine:Lysine Cross-Links. *Chem. - Eur. J.* **2017**, *23*, 5804−5813.
(24) Ye, Y.; Munk, B. H.; Muller, J. G.; Cogbill, A.; Burrows, C. J.; Schlegel, H. B. Mechanistic Aspects of the Formation of Guanidinohydantoin from Spiroiminodihydantoin under Acidic Conditions. *Chem. Res. Toxicol.* **2009**, *22*, 526−535.
(25) Dumont, E.; Grüber, R.; Bignon, E.; Morell, C.; Moreau, Y.; Monari, A.; Ravanat, J.-L. Probing the Reactivity of Singlet Oxygen with Purines. *Nucleic Acids Res.* **2016**, *44*, 56−62.
(26) Dumont, E.; Grüber, R.; Bignon, E.; Morell, C.; Aranda, J.; Ravanat, J.-L.; Tuñón, I. Singlet Oxygen Attack on Guanine: Reactivity and Structural Signature within the B-DNA Helix. *Chem. - Eur. J.* **2016**, *22*, 12358−12362.
(27) Song, B.; Zhao, J.; Griesser, R.; Meiser, C.; Sigel, H.; Lippert, B. Effects of (N7)-Coordinated Nickel(II), Copper(II), or Platinum(II) on the Acid-Base Properties of Guanine Derivatives and Other Related Purines. *Chem. - Eur. J.* **1999**, *5*, 2374−2387.
(28) Saigusa, H.; Urashima, S.-h.; Asami, H. IR-UV Double Resonance Spectroscopy of the Hydrated Clusters of Guanosine and 9-Methylguanine: Evidence for Hydration Structures Involving the Sugar Group. *J. Phys. Chem. A* **2009**, *113*, 3455−3462.
(29) Blackburn, G. M.; Gait, M. J.; Loakes, D.; Williams, D. M. *Nucleic Acids in Chemistry and Biology*; Royal Society of Chemistry: Cambridge, UK, 2006.
(30) Domínguez-Martín, A.; Johannsen, S.; Sigel, A.; Operschall, B. P.; Song, B.; Sigel, H.; Okruszek, A.; González-Pérez, J. M.; Niclós-Gutiérrez, J.; Sigel, R. K. O. Intrinsic Acid-Base Properties of a Hexa-2′-Deoxynucleoside Pentaphosphate, d(ApGpGpCpCpT): Neighboring Effects and Isomeric Equilibria. *Chem. - Eur. J.* **2013**, *19*, 8163−8181.
(31) Foote, C. S. Mechanisms of Photosensitized Oxidation. *Science* **1968**, *162*, 963−970.
(32) Martinez, G. R.; Ravanat, J.-L.; Medeiros, M. H. G.; Cadet, J.; Di Mascio, P. Synthesis of a Naphthalene Endoperoxide as a Source of ^{18}O-Labeled Singlet Oxygen for Mechanistic Studies. *J. Am. Chem. Soc.* **2000**, *122*, 10212−10213.
(33) Seliger, H. H. A Photoelectric Method for the Measurement of Spectra of Light Sources of Rapidly Varying Intensities. *Anal. Biochem.* **1960**, *1*, 60−65.
(34) Khan, A.; Kasha, M. Red Chemiluminescence of Oxygen in Aqueous Solution. *J. Chem. Phys.* **1963**, *39*, 2105−2106.
(35) Liu, F.; Lu, W.; Fang, Y.; Liu, J. Evolution of Oxidation Dynamics of Histidine: Non-Reactivity in the Gas Phase, Peroxides in Hydrated Clusters and pH Dependence in Solution. *Phys. Chem. Chem. Phys.* **2014**, *16*, 22179−22191.
(36) Liu, F.; Lu, W.; Yin, X.; Liu, J. Mechnistic and Kinetic Study of Singlet O_2 Oxidation of Methionine by On-Line Electrospray Ionization Mass Spectrometry. *J. Am. Soc. Mass Spectrom.* **2016**, *27*, 59−72.
(37) Midey, A.; Dotan, I.; Viggiano, A. A. Temperature Dependences for the Reactions of O^- and O_2^- with $O_2(a^1\Delta_g)$ from 200 to 700 K. *J. Phys. Chem. A* **2008**, *112*, 3040−3045.
(38) Fang, Y.; Liu, F.; Bennett, A.; Ara, S.; Liu, J. Experimental and Trajectory Study on Reaction of Protonated Methionine with Electronically Excited Singlet Molecular Oxygen ($a^1\Delta_g$): Reaction Dynamics and Collision Energy Effects. *J. Phys. Chem. B* **2011**, *115*, 2671−2682.
(39) Lafferty, W. J.; Solodov, A. M.; Lugez, C. L.; Fraser, G. T. Rotational Line Strengths and Self-Pressure-Broadening Coefficients for the 1.27 μm, $a^1\Delta_g$-$X^3\Sigma_g^-$, υ = 0 - 0 Band of O_2. *Appl. Opt.* **1998**, *37*, 2264−2270.
(40) Mark, L. P.; Gill, M. C.; Mahut, M.; Derrick, P. J. Dual Nano-Electrospray for Probing Solution Interactions and Fast Reactions of Complex Biomolecules. *Eur. Mass Spectrom.* **2012**, *18*, 439−466.
(41) Fisher, C. M.; Kharlamova, A.; McLuckey, S. A. Affecting Protein Charge State Distributions in Nano-Electrospray Ionization via In-Spray Solution Mixing Using Theta Capillaries. *Anal. Chem.* **2014**, *86*, 4581−4588.

DOI: 10.1021/acs.jpcb.7b09515
J. Phys. Chem. B 2018, 122, 40−53

(42) Mortensen, D. N.; Williams, E. R. Theta-Glass Capillaries in Electrospray Ionization: Rapid Mixing and Short Droplet Lifetimes. *Anal. Chem.* **2014**, *86*, 9315−9321.
(43) Wampler, F. M.; Blades, A. T.; Kebarle, P. Negative Ion Electrospray Mass Spectrometry of Nucleotides: Ionization from Water Solution with SF_6 Discharge Suppression. *J. Am. Soc. Mass Spectrom.* **1993**, *4*, 289−295.
(44) Fang, Y.; Liu, J. Reaction of Protonated Tyrosine with Electronically Excited Singlet Molecular Oxygen ($a^1\Delta_g$): An Experimental and Trajectory Study. *J. Phys. Chem. A* **2009**, *113*, 11250−11261.
(45) Ervin, K. M.; Armentrout, P. B. Translational Energy Dependence of $Ar^+ + XY \rightarrow ArX^+ + Y$ (XY = H_2,D_2,HD) from Thermal to 30 eV C.M. *J. Chem. Phys.* **1985**, *83*, 166−189.
(46) Chai, J.-D.; Head-Gordon, M. Long-Range Corrected Hybrid Density Functionals with Damped Atom−Atom Dispersion Corrections. *Phys. Chem. Chem. Phys.* **2008**, *10*, 6615−6620.
(47) Marenich, A. V.; Cramer, C. J.; Truhlar, D. G. Universal Solvation Model Based on Solute Electron Density and on a Continuum Model of the Solvent Defined by the Bulk Dielectric Constant and Atomic Surface Tensions. *J. Phys. Chem. B* **2009**, *113*, 6378−6396.
(48) Alecu, I. M.; Zheng, J.; Zhao, Y.; Truhlar, D. G. Computational Thermochemistry: Scale Factor Databases and Scale Factors for Vibrational Frequencies Obtained from Electronic Model Chemistries. *J. Chem. Theory Comput.* **2010**, *6*, 2872−2887.
(49) Frisch, M. J.; Trucks, G. W.; Schlegel, H. B.; Scuseria, G. E.; Robb, M. A.; Cheeseman, J. R.; Scalmani, G.; Barone, V.; Mennucci, B.; Petersson, G. A.; et al. *Gaussian 09, Revision D.01*; Gaussian, Inc: Wallingford, CT, 2013.
(50) Maranzana, A.; Ghigo, G.; Tonachini, G. Diradical and Peroxirane Pathways in the [π2 + π2] Cycloaddition Reactions of $^1\Delta_g$ Dioxygen with Ethene, Methyl Vinyl Ether, and Butadiene: A Density Functional and Multireference Perturbation Theory Study. *J. Am. Chem. Soc.* **2000**, *122*, 1414−1423.
(51) Marchetti, B.; Karsili, T. N. V. An Exploration of the Reactivity of Singlet Oxygen with Biomolecular Constituents. *Chem. Commun.* **2016**, *52*, 10996−10999.
(52) Lee, T. J.; Taylor, P. R. A Diagnostic for Determining the Quality of Single-Reference Electron Correlation Methods. *Int. J. Quantum Chem.* **1989**, *36* (S23), 199−207.
(53) Saito, T.; Nishihara, S.; Kataoka, Y.; Nakanishi, Y.; Matsui, T.; Kitagawa, Y.; Kawakami, T.; Okumura, M.; Yamaguchi, K. Transition State Optimization Based on Approximate Spin-Projection (AP) Method. *Chem. Phys. Lett.* **2009**, *483*, 168−171.
(54) Saito, T.; Nishihara, S.; Kataoka, Y.; Nakanishi, Y.; Kitagawa, Y.; Kawakami, T.; Yamanaka, S.; Okumura, M.; Yamaguchi, K. Reinvestigation of the Reaction of Ethylene and Singlet Oxygen by the Approximate Spin Projection Method. Comparison with Multireference Coupled-Cluster Calculations. *J. Phys. Chem. A* **2010**, *114*, 7967−7974.
(55) Lu, W.; Tsai, I. H.; Sun, Y.; Zhou, W.; Liu, J. Elucidating Potential Energy Surfaces for Singlet O_2 Reactions with Protonated, Deprotonated and Di-Deprotonated Cystine Using a Combination of Approximately Spin Projected Density Functional Theory and Guided-Ion-Beam Mass Spectrometry. *J. Phys. Chem. B* **2017**, *121*, 7844−7854.
(56) Ye, Y.; Muller, J. G.; Burrows, C. J. Synthesis and Characterization of the Oxidized dGTP Lesions Spiroiminodihydantoin-2′-Deoxynucleoside-5′-Triphosphate and Guanidinohydantoin-2′-Deoxynucleoside-5′-Triphosphate. *J. Org. Chem.* **2006**, *71*, 2181−2184.
(57) Fleming, A. M.; Armentrout, E. I.; Zhu, J.; Muller, J. G.; Burrows, C. J. Spirodi(iminohydantoin) Products from Oxidation of 2′-Deoxyguanosine in the Presence of NH_4Cl in Nucleoside and Oligodeoxynucleotide Contexts. *J. Org. Chem.* **2015**, *80*, 711−721.
(58) Luo, W. M.; Muller, J. G.; Rachlin, E. M.; Burrows, C. J. Characterization of Spiroiminodihydantoin as a Product of One-Electron Oxidation of 8-Oxo-7,8-Dihydroguanosine. *Org. Lett.* **2000**, *2*, 613−616.
(59) Psciuk, B. T.; Schlegel, H. B. Computational Prediction of One-Electron Reduction Potentials and Acid Dissociation Constants for Guanine Oxidation Intermediates and Products. *J. Phys. Chem. B* **2013**, *117*, 9518−9531.
(60) Jang, Y. H.; Goddard, W. A., III; Noyes, K. T.; Sowers, L. C.; Hwang, S.; Chung, D. S. Pka Values of Guanine in Water: Density Functional Theory Calculations Combined with Poisson-Boltzmann Continuum-Solvation Model. *J. Phys. Chem. B* **2003**, *107*, 344−357.
(61) Podolyan, Y.; Gorb, L.; Leszczynski, J. Protonation of Nucleic Acid Bases. A Comprehensive Post-Hartree-Fock Study of the Energetics and Proton Affinities. *J. Phys. Chem. A* **2000**, *104*, 7346−7352.
(62) Luo, W.; Muller, J. G.; Rachlin, E. M.; Burrows, C. J. Characterization of Hydantoin Products from One-Electron Oxidation of 8-Oxo-7,8-Dihydroguanosine in a Nucleoside Model. *Chem. Res. Toxicol.* **2001**, *14*, 927−938.
(63) Steinfeld, J. I.; Francisco, J. S.; Hase, W. L. *Chemical Kinetics and Dynamics*, 2nd ed.; Prentice Hall: Upper Saddle River, NJ, 1999.
(64) Abel, E. Über Einen Besonders Einfachen Fall von Stufenreaktionen. *Z. Phys. Chem.* **1906**, *56U*, 558−564.
(65) Alshykhly, O. R.; Fleming, A. M.; Burrows, C. J. 5-Carboxamido-5-Formamido-2-Iminohydantoin, in Addition to 8-Oxo-7,8-Dihydroguanine, Is the Major Product of the Iron-Fenton or X-Ray Radiation-Induced Oxidation of Guanine under Aerobic Reducing Conditions in Nucleoside and DNA Contexts. *J. Org. Chem.* **2015**, *80*, 6996−7007.
(66) Fleming, A. M.; Muller, J. G.; Ji, I.; Burrows, C. J. Characterization of 2′-Deoxyguanosine Oxidation Products Observed in the Fenton-Like System Cu(II)/H_2O_2/Reductant in Nucleoside and Oligodeoxynucleotide Contexts. *Org. Biomol. Chem.* **2011**, *9*, 3338−3348.
(67) Ye, W.; Sangaiah, R.; Degen, D. E.; Gold, A.; Jayaraj, K.; Koshlap, K. M.; Boysen, G.; Williams, J.; Tomer, K. B.; Mocanu, V.; Dicheva, N.; Parker, C. E.; Schaaper, R. M.; Ball, L. M. Iminohydantoin Lesion Induced in DNA by Peracids and Other Epoxidizing Oxidants. *J. Am. Chem. Soc.* **2009**, *131*, 6114−6123.
(68) Ravanat, J.-L.; Saint-Pierre, C.; Di Mascio, P.; Martinez, G. R.; Medeiros, M. H. G.; Cadet, J. Damage to Isolated DNA Mediated by Singlet Oxygen. *Helv. Chim. Acta* **2001**, *84*, 3702−3709.
(69) Martinez, G. R.; Loureiro, A. P. M.; Marques, S. A.; Miyamoto, S.; Yamaguchi, L. F.; Onuki, J.; Almeida, E. A.; Garcia, C. C. M.; Barbosa, L. F.; Medeiros, M. H. G.; Di Mascio, P. Oxidative and Alkylating Damage in DNA. *Mutat. Res., Rev. Mutat. Res.* **2003**, *544*, 115−127.
(70) Weimann, A.; Belling, D.; Poulsen, H. E. Quantification of 8-Oxo-Guanine and Guanine as the Nucleobase, Nucleoside and Deoxynucleoside Forms in Human Urine by High-Performance Liquid Chromatography-Electrospray Tandem Mass Spectrometry. *Nucleic Acids Res.* **2002**, *30*, e7.
(71) Truhlar, D. G.; Garrett, B. C.; Klippenstein, S. J. Current Status of Transition-State Theory. *J. Phys. Chem.* **1996**, *100*, 12771−12800.

DOI: 10.1021/acs.jpcb.7b09515
J. Phys. Chem. B 2018, 122, 40−53